Université d'Ottawa · University of Ottawa

To my dear mother and father,
and to my brothers for believing in me...

To those who will breach the ultimate barriers of space travel...

Acknowledgments

I would like to express my gratitude to my supervisor, Dr. Mario Morin for his guidance throughout my research project and for teaching me all that I know about conducting research independently. I thank all my colleagues, Hassan Al-Maznai, Deyu Qu, Dr. Nadereh Mohtat, Dr. Dongfang Yang and Sandra Rifai for their support in the laboratory, many useful discussions, and the great fun that we had working together. I am grateful to Mark Soucy, a good friend, for his support and good sense of humor during my research project. I also acknowledge my mother, father, and brothers for their tremendous support. Finally I would like to thank the government of Ontario for a postgraduate scholarship.

Abstract

We present a spectroelectrochemical study of the reductive desorption and the oxidative redeposition of a monolayer of 1-hexadecanethiols on Au(111) in an aqueous alkaline electrolyte solution. The solvent/thiol interactions were found to play an important role in the electrodeposition of self-assembled monolayers of low-solubility thiols. Ex situ vibrational spectroscopy shows that the orientation of the alkane chains in a monolayer remains unchanged after its reductive desorption and oxidative redeposition. In situ spectroelectrochemical measurements reveal that the reductive desorption/oxidative redeposition of low-solubility thiols on Au(111) proceed through a two step mechanism. The first step of the reductive desorption is ascribed to the reduction of chemisorbed thiols. The thiolates formed remain physisorbed in a lamellar arrangement. The second step of the reductive desorption occurs at a more negative potential and is assigned to the reorientation of the monolayer of physisorbed thiolates into micelles. The unblocking of the Au(111) surface caused by this reorientation of the thiolates allows the formation of an electrical double layer. This gives rise to a capacitive current. The oxidative redeposition proceeds by these two steps in the reverse order. If the reduced thiolates remain physisorbed for more than 3 minutes, a slow stabilization of the physisorbed state occurs to make it more difficult to oxidatively redeposit the thiolates. This stabilization is ascribed to a slow protonation of the thiolates. In situ SHG spectroscopy signals were used to follow the reductive desorption and the oxidative redeposition. For potential steps to very negative or positive potentials, the SHG signal changes with the charge variation observed for the reductive and oxidative potential steps. For reductive potential steps to less negative values, the kinetics of the reduction are slower and can be monitored via SHG spectroscopy. The slow stabilization of physisorbed thiolates has been monitored using time-resolved SHG spectroscopy.

These SHG measurements support the stabilization of physisorbed thiolates by a protonation process. The thiols are less polarizable and this causes important variations of the SHG signal intensity.

List of Figures

V and - 1.20 V. Each data point is an average of three measurements. Each measurement is an average of 200

spectra recorded at a resolution of 2 cm^{-1}. See the text for more details.

Figure 3.8 (p. 47): Proposed model for the repetitive reductive desorption/oxidative redeposition of a chemisorbed monolayer of low-solubility thiols. The reduction proceeds through the following steps: (a) chemisorbed thiols; (b) the reduction of the chemisorbed thiols creates the physisorbed thiolates, which form a lamellar structure; (c) when the potential is made more negative, physisorbed micelles of thiolates are formed. The oxidative redeposition proceeds through the reverse order of these steps.

Figure 4.1 (p. 52): Changes in the stability of physisorbed C16 thiolates on Au(111) with time. The cyclic voltammograms were recorded as follows. The potential was scanned from - 0.30 V to - 1.30 V to reduce the C16 monolayer. On the subsequent positive scan, the potential was held at - 1.10 V for 1, 5, and 15 minutes before recording the oxidative redeposition.

Figure 4.2 (p. 59): % variation of the SHG signal intensity with time for: (a) to (e): the reduction and the oxidation of C16 on Au(111). The reductive potential steps (A) were from - 0.30 V to (a) - 1.12 V, (b) - 1.14 V, (c) - 1.16 V, (d) - 1.18 V, and (e) - 1.20 V. In each case, we waited 3 minutes before jumping back to - 0.30 V (B). (f): the reduction and the oxidation of C4 on Au(111). The reductive potential step (A) was from - 0.30 V to - 1.00 V. We waited 3 minutes before jumping back to - 0.30 V (B). (g): a blank experiment. The potential of a clean Au(111) surface was jumped from - 0.30 V to - 1.20 V (A), and held at - 1.20 V for 3 minutes. Then, the potential was jumped back to

- 0.30 V (B). Each trace ((a) to (g)) is an average of 10 measurements. Each data point of the individual traces used for signal averaging is an average of 10 sums of 5 laser shots.

Figure 4.3 (p. 62): Cyclic voltammogram obtained when the Au(111) surface is immersed in an electrolyte solution of 0.1 M KOH containing 10 mM of 1-butanethiolates. The scan rate was 20 mV s^{-1}.

Figure 4.4 (p. 66): % variation of the SHG signal intensity with time for a blank experiment. The potential of a clean Au(111) surface was jumped from - 0.30 V to - 1.20 V (A) and held at - 1.20 V for 15 minutes. Then it was jumped back to - 0.30 V (B). Each data point in the SHG signal trace is an average of 10 sums of 10 laser shots.

Figure 4.5 (p. 67): % variation of the SHG signal intensity with time for the reduction and the oxidation of C16 on Au(111). The reductive potential step (A) was from - 0.30 V to - 1.20 V. We waited 30 minutes before jumping back to - 0.30 V (B). Each data point in the SHG signal trace is an average of 10 sums of 10 laser shots.

Figure 4.6 (p. 69): % variation of the SHG signal intensity with time for the reduction and the oxidation of C16 on Au(111). The reductive potential step (A) was from - 0.30 V to - 1.22 V. We waited 30 minutes before jumping back to - 0.30 V (B). Each data point in the SHG signal trace is an average of 10 sums of 10 laser shots.

Figure 4.7 (p. 70): % variation of the SHG signal intensity with time for the reduction and the

oxidation of C16 on Au(111). The reductive potential step (A) was from - 0.30 V to - 1.22 V. We waited 30 minutes before jumping back to - 0.30 V (B). Each data point in the SHG signal trace is an average of 10 sums of 10 laser shots.

Figure 4.8 (p. 71): % variation of the SHG signal intensity with time for the reduction and the oxidation of C16 on Au(111). The reductive potential step (A) was from - 0.30 V to - 1.14 V. We waited 30 minutes before jumping back to - 0.3 V (B). Each data point in the SHG signal trace is an average of 10 sums of 10 laser shots.

Figure 4.9 (p. 73): % variation of the SHG signal intensity with time for the reduction and the oxidation of C4 on Au(111). The reductive potential step (A) was from - 0.30 V to - 1.00V. We waited 15 minutes before jumping back to - 0.30 V (B). Each data point in the SHG signal trace is an average of 10 sums of 10 laser shots.

Figure 4.10 (p. 74): % variation of the SHG signal intensity with time for the reduction and the oxidation of C4 on Au(111). The reductive potential step (A) was from - 0.30 V to - 1.20 V. We waited 30 minutes before jumping back to - 0.30 V (B). Each data point in the SHG signal trace is an average of 10 sums of 10 laser shots.

Figure 4.11 (p. 75): % variation of the SHG signal intensity with time for the reduction and the oxidation of C4 on Au(111). The reductive potential step (A) was from - 0.30 V to - 1.22 V. We waited 30 minutes before jumping back to - 0.30 V (B). Each data point in the SHG signal trace is an average of 10 sums of 10 laser shots.

Figure 5.1 (p. 82): Proposed model for the repetitive reductive desorption/oxidative redeposition of a chemisorbed monolayer of low-solubility thiols. The reduction proceeds through the following steps: (a) chemisorbed thiols; (b) the reduction of the chemisorbed thiols creates the physisorbed thiolates, which form a lamellar structure; (c) when the potential is made more negative, physisorbed micelles of thiolates are formed. If we maintain the thiolates in the micellar state (c), a reversible protonation occurs after 3 minutes. The oxidative redeposition proceeds through the reverse order of these steps.

Table of Contents

CHAPTER 3: In situ Vibrational Spectroscopy Results

CHAPTER 4: SHG Spectroscopy Results

CHAPTER 5: Conclusion

CHAPTER 1: Introduction

Recently, it was found that ordered organic interfaces of molecular dimensions could be formed by simple chemical processes. Potential applications of such interfaces are numerous. Particularly, the self-assembly of thiols onto gold metal surfaces was found to modify the electrochemical, physical, and optical (shown in this study) properties of the metal.

The adsorption of alkanethiols onto gold substrates from a solution is an exothermic (~ 160 - 190 kJ/mol) [1,2] process that is governed by the strong affinity of the sulfur head group for gold and the nature of the solvent/alkanethiol interactions. The thiols occupy preferential binding sites of 3-fold symmetry separated by 5 Å. The close-packed arrangement of thiols that results from this chemisorption process allows for short range Van der Waals interactions between the alkyl chains. The alkyl chains orient themselves in order to optimize favourable chain-chain interactions and the interactions between the chains and the interfacial environment (exothermic by $\leq$ 40 kJ/mol) [1,3]. This spontaneous organization of the alkyl chains is called self-assembly. Self-assembly is a slow process which depends on the inter-adsorbate distance, the structure of the adsorbate, and the nature of the solvent [1,4]. The entropy decreases during these self-assembly processes. Hence the formation of self-assembled monolayers is not favourable from an entropic point of view. However, the highly exothermic chemisorption of thiols onto gold and the resulting close-packed arrangement of the thiols (short inter-adsorbate distances) make self-assembly a thermodynamically driven process.

The monolayers that results from the self-assembly of alkanethiols on gold substrates have a high degree of order. The crystalline quality of an alkanethiol monolayer covering gold confers to the

metal surface resistance to mechanical wear (friction) [1]. The low dielectric constants of alkane chains, their close-packing arrangement and the physical separation they provide between the metal surface and its envrironment confers to these monolayers the ability to screen the electric field felt by interfacial charges when a potential is applied to the metal. This property was used in the development of biosensors for the medical environment [5,6] and may be used as a corrosion inhibition technique [1]. As we will see in this study, the nonlinear optical properties of a gold surface are modified by the presence of a self-assembled monolayer of alkanethiols. Thus, these alkanethiol/gold systems present some potential as optical switches. The electrochemical properties of strongly hydrophobic alkanethiol monolayers on gold presents some potential in the development of molecular switches.

The success of the applications mentioned above depends on the quality (homogeneity: low number of defects in the monolayer) of the alkanethiol monolayers formed. Consequently, the success of these applications depends on our ability to control the quality of self-assembled monolayers. In this respect, it is imperative that we possess a good understanding of how self-assembled monolayers are formed and how we may control their quality.

Self-assembled monolayers of thiols are usually deposited onto metal substrates by incubating the substrate in a solution containing thiols [3,7]. This method of deposition, although very simple, has disadvantages. The choice of the solvent, the solubility, and the concentration of the thiol are crucial parameters that must be balanced properly in order to form high quality self-assembled monolayers. The formation of self-assembled monolayers from a solution is slow. It requires incubating the metal substrate in the solution for hours to days [3,7-9]. An in situ verification of the cleanliness of the

metal substrate's surface is not possible. Surface cleanliness is important since it has been shown to influence the quality and the stability of a monolayer [10]. In summary, this method of deposition does not provide a good control of the quality of self-assembled monolayers. Alternatively, we may deposit self-assembled monolayers of thiols electrochemically. This is done by immersing the metal substrate in an alkaline solution containing thiolates [11-14]. A monolayer of thiolates oxidatively deposits onto the metal surface when a sufficiently positive potential is applied to the substrate. Compared with the incubation method, this only takes a few seconds. The rapidity of this deposition method does not compromise the quality of the self-assembled monolayers. The electrodeposited monolayers have the same surface coverage, structure, and electrochemical properties as the monolayers obtained via the incubation method. The electrochemical deposition method also allows the in situ cleaning of the substrate prior to the deposition of a monolayer. Finally, submonolayer coverages of thiols may be acheived by properly selecting the potential value and the time spent at this potential. Thus, the electrochemical deposition method provides more control of the quality of self-assembled monolayers of thiols.

The electrodeposition of ethanethiolates from alkaline solutions has been investigated on Au [11], Ag [12,13], and Hg [14] substrates. The ethanethiolates were found to oxidatively adsorb onto annealed Ag(111) films and Hg via a two step process [12-14]. The formation of a low-coverage phase via a Langmuir process characterizes the first step. Then, ethanethiolate islands grow from the nucleation centers established in the first step to produce a high-coverage phase. The low and high coverage phases on Ag were characterized by Raman spectroscopy. This revealed that the alkane chains of the ethanethiolates exhibit gauche defects in the low-coverage phase and an all-trans configuration in the high-coverage phase. The gauche defects disappeared upon the formation of the

high-coverage phase. An electrosorption valency of one was found for the oxidative adsorption of ethanethiolates on Ag. On the other hand, the electrodeposition of ethanethiolates on Au(111) occurs in one step [11]. This is shown by the presence of only one symmetric current peak in the oxidative adsorption voltammograms. The origin of these different mechanisms is unclear.

The electrodeposition of thiols is not only dependent on the nature of the substrate. The interactions among thiols, between the thiols and the solvent, and the choice of the electrolyte solution also influence the process of electrodeposition. Consequently, solubility is an important parameter in the electrodeposition of thiolates. If we carry out the electrodeposition of thiolates in a non-polar solvent, where they are very soluble, a low surface coverage is observed [15]. In aqueous electrolyte solutions, when the alkane chain length of thiolates increases, their solubility decreases. This decrease of solubility is accompanied by changes in the reductive desorption voltammogram of the thiolates. Particularly, on Au(111) single crystals, the reductive desorption voltammogram of a monolayer of chemisorbed thiols with an alkane chain length greater than 12 carbons exhibits two current peaks [16]. Only one current peak is observed when the alkane chain length is equal to or less than 12 carbons [16-18]. Two models have been proposed to account for the appearance of the two current peaks in the reductive desorption voltammograms of low-solubility thiols chemisorbed on Au(111) [16,17]. One model suggests the presence of two domains with different packing densities. The difference in the ionic permeability between these two domains would cause the thiols of each domain to reductively desorb at different potentials. The other model ascribes the two reductive peaks to the reductive desorption of thiols from two different adsorption sites. The increase in the inter-adsorbate interactions would cause thiols to adsorb on three fold sites and on top sites, a configuration which would allow for a greater packing density. However, there is no evidence to support either model.

Because of their very low solubility in aqueous electrolyte solutions, long chain thiols such as hexadecanethiols remain physisorbed on the substrate's surface after their reductive desorption, most probably in the form of micelles [16,17]. Thus, the same monolayer can be reductively desorbed and oxidatively adsorbed repetitively. The chemisorbed monolayer resulting from this treatment remains well-ordered. An understanding of the mechanism of the oxidative adsorption/reductive desorption of low-solubility thiols should improve our ability to make high quality self-assembled monolayers.

This thesis presents a spectroelectrochemical study of a self-assembled 1-hexadecanethiol (C16) monolayer chemisorbed on a Au(111) single crystal substrate. We found that the decrease of the solubility of the alkanethiols with the increase in the number of carbon atoms in the chain is responsible for the presence of two current peaks in the voltammetric waves of the reductive desorption and the oxidative adsorption of C16 on Au(111). A new model is presented for the electrodeposition of low-solubility thiols. It consists of the electrospreading of physisorbed micelles of thiolates. Whenever a C16 monolayer is held in its physisorbed state for longer than 3 minutes, the physisorbed thiolates undergo a slow reversible stabilization which makes the subsequent electrodeposition more difficult.

The thesis opens with a Theory and Experiment chapter that presents the theory used to analyze the experiments and the details of the procedures, instruments, and chemicals used in the experiments. The spectroelectrochemical study is presented in two separate chapters. Chapter 3 deals with our in situ FTIR spectroscopy results, on the basis of which a new model is presented for the electrodeposition of low-solubility thiols. Chapter 4 presents our SHG spectroscopy results. To the extent of the knowledge of the author, SHG spectroscopy is used for the first time to study the

reductive desorption and the oxidative redeposition of an organic adsorbate. The use of SHG spectroscopy was prompted by electrochemical evidence of the stabilization of physisorbed C16 thiolates with time and the insensitivity of in situ FTIR spectroscopy to this process. The insensitivity of in situ FTIR spectroscopy to the stabilization of physisorbed C16 thiolates is an indication that there are no significant changes in the orientation of the physisorbed thiolates during this process. Thus, the stabilization process must be due to a reorganization of the electronic density distribution at the surface of the substrate. SHG spectroscopy is particularly sensitive to changes in the electronic density distribution at metal substrate surfaces [19]. In this respect, the technique has been employed on many occasions to study the kinetics of the spontaneous adsorption of thiols from a solution [4,20,21]. Finally, Chapter 5 gives the concluding remarks.

CHAPTER 2: Theory and Experiment

Each section in this chapter is composed of two parts. The first part introduces the essential theory behind an experimental technique that was used to study the reductive desorption and the oxidative redeposition of C16 on Au(111). The second part presents a description of the procedures, instruments, and chemicals pertaining to the experimental technique.

2.1 Cylic voltammetry:

Theory:

Cyclic voltammetry consists in applying a linear potential sweep cycle to an electrode between two preset limits of potential, and measuring the resulting current developed on this electrode. Two kinds of currents can be measured. The faradaic current is due to an electron transfer process across the electrode/solution interface. The nonfaradaic current is ascribed to the adsorption or the desorption of species at the electrode/solution interface without charge transfer. If we assume the nonfaradaic current to be similar to that of an RC circuit we have:

$$i(t) = \nu C_d + \left[\left(\frac{E_i}{R_s} - \nu C_d\right)\exp\left(-\frac{t}{R_s C_d}\right)\right] \qquad (2.1)$$

i = capacitive current (μA), ν = linear potential sweep rate (mV/s); constant through time, C_d = capacitance of the electrode/electrolyte interface or double layer capacitance (μF), E_i = potential at which the linear potential sweep starts (V), R_s = resistance of the electrochemical circuit (Ω), and t = time (seconds). The transient current term is the second term in square brackets in equation (2.1) and it takes into account the variation of the double layer capacitance as a function of potential when

a species is being adsorbed or desorbed. The steady state term (vC_d) outside the square brackets dominates when the double layer capacitance of the system under study is very small. When a monolayer of C16 is chemisorbed on Au(111), the capacitance is very small and we may describe the current with the following equation:

$$i = vC_d \qquad (2.2)$$

However, when the C16 monolayer gets reductively desorbed or oxidatively redeposited, equation (2.1) must be used to describe the nonfaradaic (or capacitive) current. Thus the total current for these processes is the sum of the capacitive part (formation of an electrical double layer; see Figure 2.1) plus the faradaic part (reduction/oxidation of C16; electron transfer). These two parts are normally coupled for species that undergo rapid mass transfer between the bulk electrolyte solution and the surface of the electrode when they are reduced/oxidized. However, in some cases they may be decoupled due to the nature of the adsorbate. We will see that for C16 on Au(111), the reductive desorption and the oxidative redeposition currents are described by the sum of the capacitive and faradaic parts and that these currents are decoupled (i.e. resolved) due to the low-solubility of this adsorbate.

Experimental:

Cyclic voltammetry was performed with a three-electrode potentiostat/galvanostat (Pine Instruments Co., model AFRDE5) connected to a computer for digital acquisition of the cyclic voltammograms. The working electrode was a Au(111) single crystal. The counter electrode was either a gold wire (99.999 % Engelhard), 0.5 mm in diameter and shaped into a coil, or a platinum foil (99.999 % Engelhard) shaped into a ring. The reference electrode was a saturated calomel electrode. All the potentials given in this paper are relative to a saturated calomel electrode (SCE). The potential scan rate used to record the cyclic voltammograms was 20 mV s^{-1}. All measurements

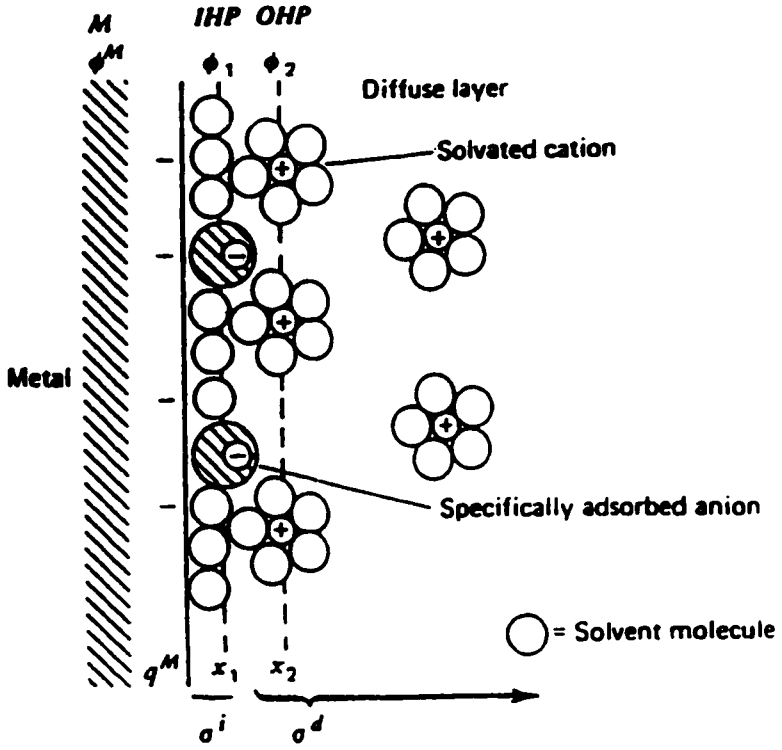

Figure 2.1: A model of the electrical double layer. σ^i is the charge density from ions in the inner Helmholtz plane (IHP). σ^d is the charge density from ions in the outer Helmholtz plane (OHP).

(taken from ref. 47)

were done in 0.1 M KOH (Aldrich, semiconductor grade) made with deionized distilled water (Milli-Q, Millipore). The electrolyte was prepared from a concentrated (18 M) KOH stock solution. Then it was standardized and kept in a sealed teflon bottle. Thus, the same electrolyte solution could be used for a whole week with less than 0.7 % change in the concentration throughout the period of use. The electrolyte solutions were degassed with Ultra Pure Carrier argon gas (Air Products Canada) or nitrogen (departmental line nitrogen further purified with a filter to remove traces of O_2 and H_2O) prior to the measurements. The cyclic voltammograms were measured after lifting up the Au(111) single crystal above the surface of the solution in order to form a hanging meniscus such that only the (111) surface is in contact with the electrolyte. Charge densities were obtained via a numerical integration of the current measured in the voltammograms. 1-Hexadecanethiols were purchased from Aldrich and used as received. The monolayers were chemically deposited onto the Au(111) surface by first annealing the electrode in a natural gas flame and then incubating it in a 10 mM ethanolic solution (Omnisolv, spectroscopic grade ethanol) of 1-hexadecanethiols for 1 hour.

Two kinds of cells were used to perform the electrochemistry. The electrochemical cell (see Figure 2.2) was used whenever we had to integrate the current in the voltammograms to obtain charge densities. Shown in Figure 2.3 is the cell that we designed for our spectroelectrochemical measurements. Both cells were made of pyrex glass. Before each experiment, the cells were immersed in boiling concentrated sulfuric acid (BDH) for 15 - 30 minutes to destroy any organic impurities. Milli-Q water was used to rinse away the sulfuric acid. After this treatment, the cells were immediately rinsed and filled with a 0.1 M KOH solution. In the case of the electrochemical cell, the counter electrode was the gold wire in the shape of a coil. This electrode was flame-annealed to burn off organic impurities prior to its insertion in the electrochemical cell. The optical windows of the

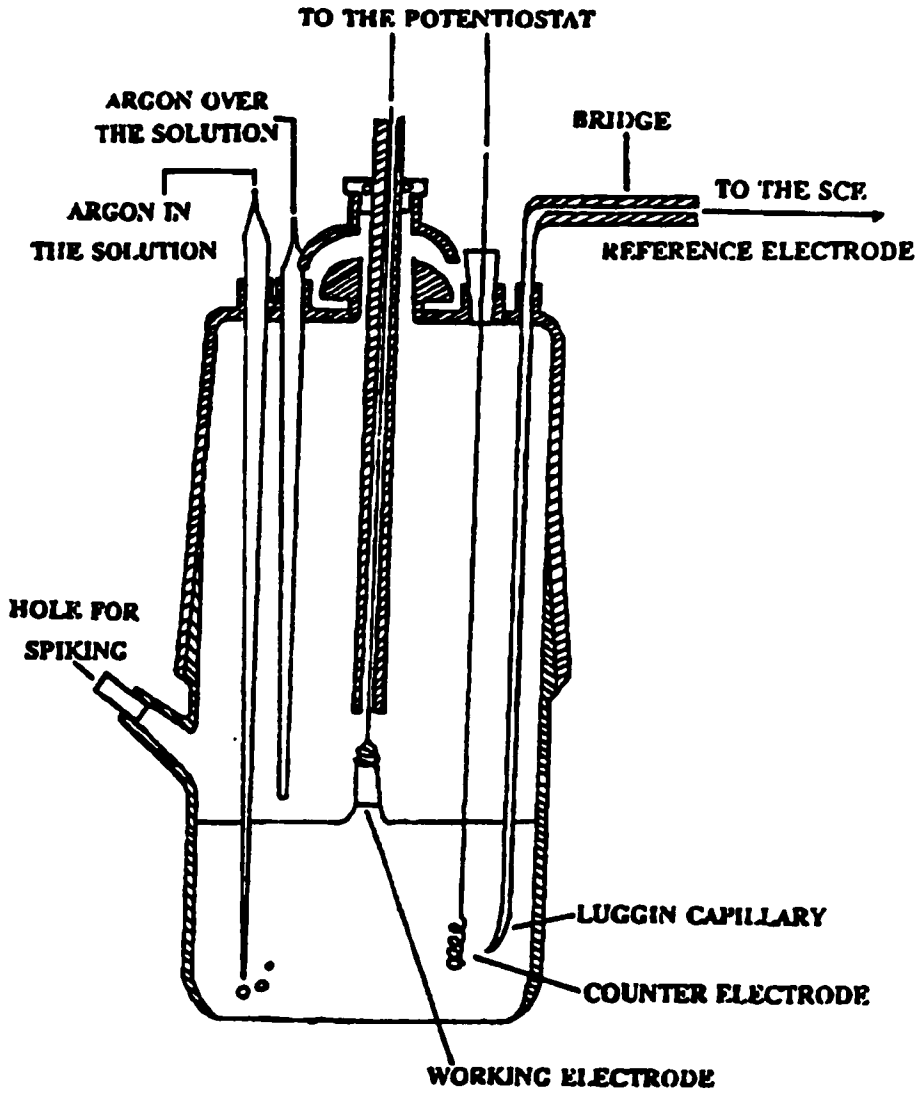

Figure 2.2: The electrochemical cell.

(taken from ref. 48)

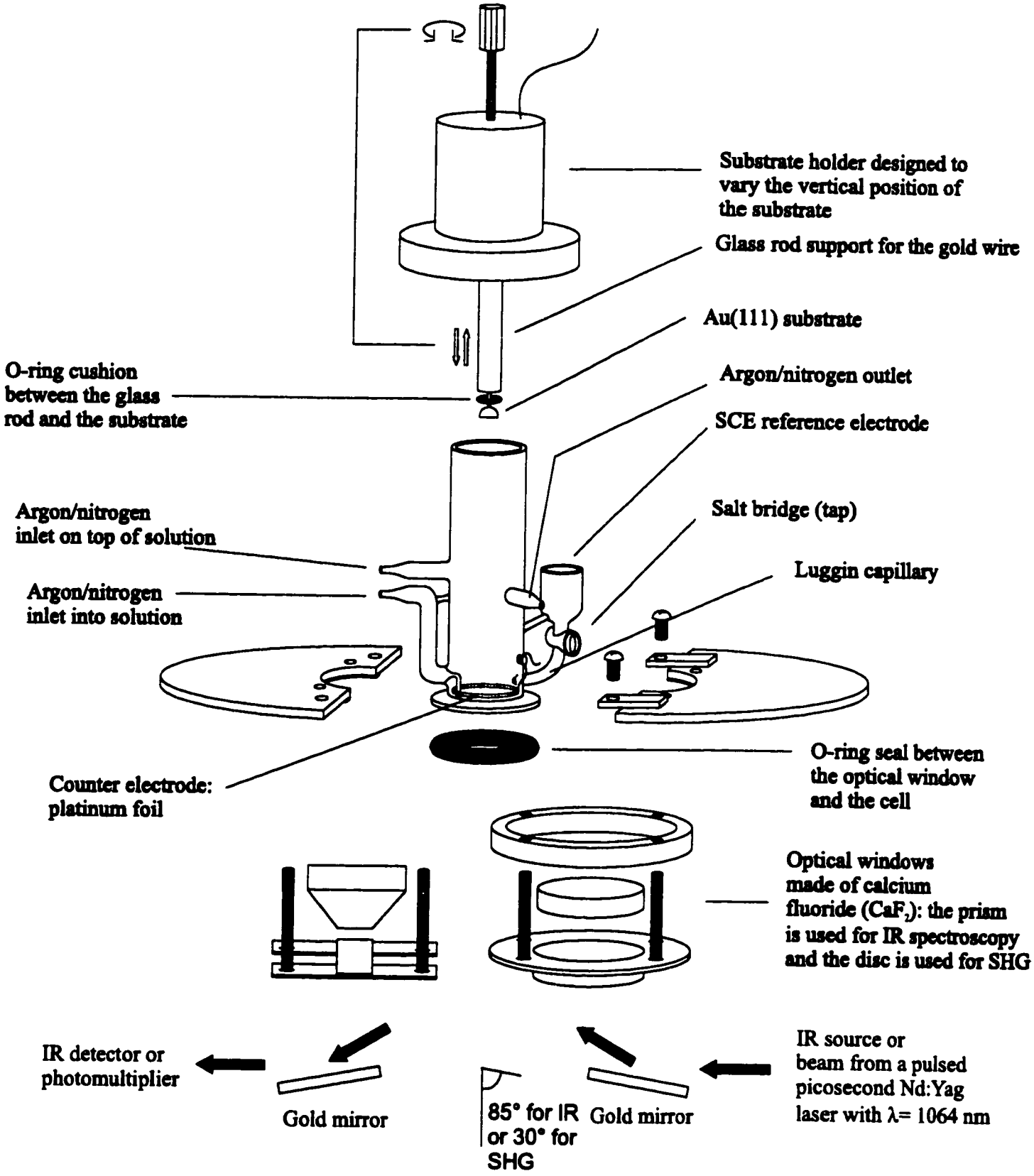

Figure 2.3: The spectroelectrochemical cell.

spectroelectrochemical cell were cleaned by ample rinsing with Omnisolv ethanol and Milli-Q water. The o-rings for the spectroelectrochemical cell were cleaned by immersion in concentrated sulfuric acid for 30 seconds and ample rinsing with Milli-Q water. The cleanliness of the cells was verified by recording a cyclic voltammogram between - 1.10 V and + 0.45 V in 0.1 M KOH. The experiments were carried out only when the voltammogram was identical to previous reports [22].

2.2 Au(111) single crystal preparation:

Theory:

Surface processes (adsorption, desorption, and surface reactions) are greatly dependent on the crystallographic orientation of a substrate. Different crystallographic orientations present different surface structures and frontier molecular orbitals, hence different reactivities. This makes the mechanistic studies of surface processes on polycrystalline substrates difficult. Consequently, the use of single crystal substrates is more common since it simplifies the analysis of the results. Between the different crystallographic orientations of a single crystal substrate, there may be a preferred orientation for the type of surface process that is to be studied. For the study of the reductive desorption and the oxidative redeposition of low-solubility thiols (eg. C16) on gold, the (111) orientation is preferred. Between the most commonly used low index orientations of single crystal gold, (100), (110), and (111), (111) has the most positive pzc (potential of zero charge). This ensures that the large overpotentials required to reductively desorb low-solubility thiols will be before the (less negative) hydrogen evolution. Self-assembled monolayers of thiols on Au(111) also have a higher packing density. In this respect, low-solubility thiols/Au(111) systems present a number of interesting physical and chemical properties of practical importance (see CHAPTER 1).

Experimental:

The Au(111) single crystal electrode was made from pure gold (99.999 %, Engelhard). An induction furnace (Elma Engineering, California) was used to melt the crystal into the form of a bead. The single crystal was oriented to within ± 0.5° of the (111) plane in a goniometer using van Laüe X-ray back reflection. The cutting of the single crystal along the (111) plane and the first part of the mechanical polishing were done with different grades of waterproof Si-Carbide polishing paper (Tech-Met Canada and Struers). The polishing was continued on polishing cloths (Technotron cloth, Leco) using 6 μm, 1 μm, and 0.1 μm diamond suspensions (Metadi, Buehler). The geometrical area of the resulting Au(111) surface was 0.70 cm^2. The mechanical polishing was followed by an electrochemical polishing to get rid of microscopic defects. This was done via the galvanostatically controlled oxidation of the Au(111) surface in 1 M $HClO_4$ (Seastar Chemicals, Vancouver, Canada). Finally, the Au(111) electrode was flame annealed in a natural gas flame at the begining of each experiment to relieve the stress in the metal and burn off any organic impurities. The quality and the cleanliness of the Au(111) electrode were checked by recording a cyclic voltammogram in a 0.1 M $HClO_4$ solution and comparing it to previous reports [23]. In this electrolyte, the cyclic voltammogram provides finger prints for the different crystallographic orientations due to the sensitivity of this technique to different crystallographic orientations. Our voltammogram was indentical to previous reports. Additional details for the preparation of Au(111) single crystals are provided elsewhere [23, 24].

2.3 Ex situ IR spectroscopy (Reflection-Absorption FTIR spectroscopy):

Theory:

In RA FTIR spectroscopy, a monolayer coated metal surface reflects an incident beam of infrared

radiation onto a detector. The light components of the incident beam which disappear in the reflected beam are absorbed by the species present on the metal surface. This absorption phenomenon is governed by the selection rule arising at metal surfaces [25]. It follows from this rule that: 1) only the transition dipoles (electric dipole variation) or components of the transition dipoles perpendicular to the surface, contribute to the absorption of the incident light, 2) the absorption is more intense when the angle between the incident beam and the surface normal is large (when the grazing angle is large), 3) the absorption phenomenon only takes place with the component of incident light that is perpendicular to the plane of the surface. The selection rule is rationalized by considering what happens to electric dipoles (of the surface species) and the electric fields (oscillating electric fields of IR light) in the vicinity of a metal's surface. An electric dipole or an electric field oriented perpendicularly to the plane of a metal's surface will generate an electrical image of itself within the metal surface. This electrical image will have the same vectorial orientation as the electric dipole or the electric field which induced it; the electrical image is also said to be in phase with its corresponding electric dipole or electric field. A reinforcement of the electric dipole or the electric field will occur as a result of adding its associated vector to that of the electrical image. An electric dipole or an electric field which is parallel to the plane of a metal's surface will generate an antisymmetric electrical image of itself. The result is then a vectorial cancellation of the electric dipole or the electric field with its electrical image as shown in Figure 2.4. Figure 2.4 also shows how the grazing angle affects the orientation of the electric field of the incident light, which in turn affects how well the incident light interacts with the perpendicular component of the transition dipoles of the species adsorbed on a metal surface. In this fashion, we may relate the intensities of the different IR bands of a species adsorbed on a metal surface to their orientations.

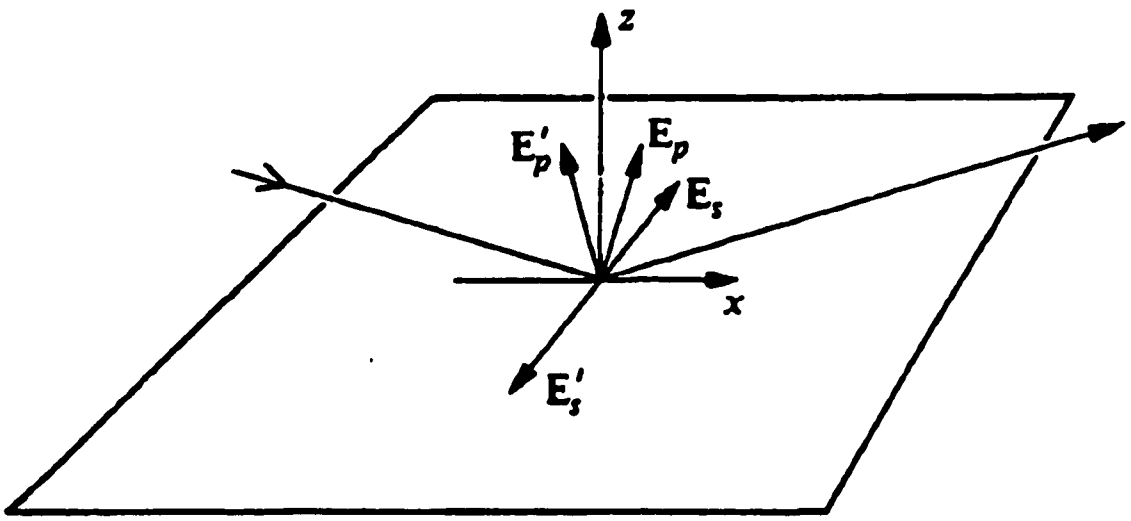

Figure 2.4: Case of the electric dipole ⊥ to the surface: E_p and E_p' represent the vectorial orientations of the net electric dipole of the incident and reflected beams of light respectively. A large grazing angle (angle between the surface normal and the incident or reflected beam of light) makes the vectors E_p and E_p' more ⊥ to the surface. Case of the electric dipole // to the surface: E_s and E_s' represent the vectorial orientations of the electric dipole and its electrical image respectively. They cancel out.

Experimental:

Ex situ infrared differential reflectance spectra were carried out using the experimental setup described in Figure 2.5. A Nicolet Magna 550 FTIR spectrometer performed the measurements under a nitrogen atmosphere. The IR radiation of the incident beam was polarized perpendicularly to the surface of the sample using a ZnSe wire grid polarizer. The gold mirrors were positioned to form a grazing angle of 80°. The intensity of the spectra is expressed in units of differential reflectance $\Delta R/R$. This is done by substracting a reference spectrum from a sample spectrum to get ΔR. ΔR is then divided by the reference spectrum, R. The choice of sample and reference spectra varied between experiments and will be specified when required for each experiment.

2.4 In situ vibrational spectroscopy (SNIFTIRS):

Theory:

In situ vibrational spectroscopy monitors the variations of the intensity of absorption of IR bands at a metal surface when the metal substrate is subjected to different electrochemical conditions. These variations are caused by the adsorption, desorption, or chemical transformation of IR active species at the metal surface. If these variations are observed only with p-polarized incident IR light, then the IR active species causing these variations are only at the metal surface. The observation of these variations with s-polarized incident IR light is indicative that the IR active species desorb from or adsorb onto, the metal surface. The selection rule is the same as described in the previous section.

Experimental:

These experiments were carried out using the same instruments as for the ex situ IR spectroscopy experiments. Our spectroelectrochemical cell was used for these experiments. Both the cell and the optical setup are described in Figure 2.3. The 60° CaF_2 trapezoidal prism was used as the optical

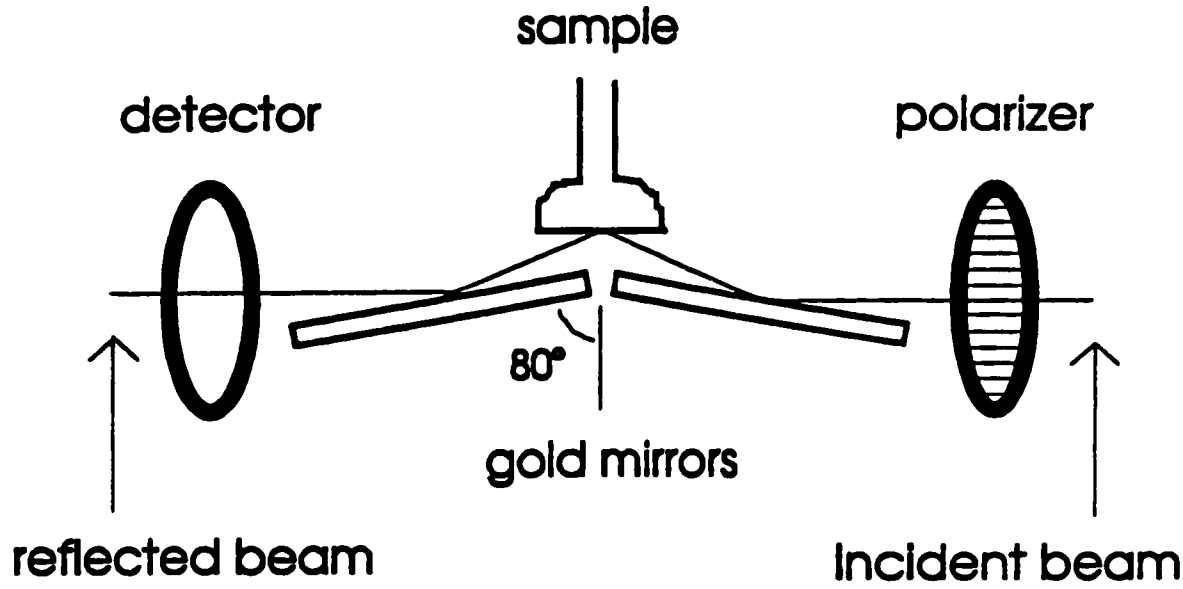

Figure 2.5: RA FTIR experimental setup scheme.

window mounted at the bottom of the cell. Thus the angle of incidence of the IR light at the electrode surface was 85 ± 5°. In this cell, the Au(111) crystal can be pressed onto the CaF_2 window to form a thin electrolyte layer of a few micrometers. This configuration decreases the contributions of IR absorption from the electrolyte in order to observe more easily the small variations of IR absorption ($\sim 10^{-3}$ $\Delta R/R$, 0.1 %) due to our electrochemically induced processes. A hanging meniscus can also be established in this cell to carry out cyclic voltammetry.

2.5 SHG spectroscopy:

Theory:

When light interacts with a macroscopic material it induces a polarization of the electrons in the material with the electric field component, **E**, of its wave. The polarization is approximated by a power series:

$$\mathbf{p} = \chi^{(1)} \bullet \mathbf{E} + \chi^{(2)} \bullet\bullet \mathbf{EE} + \chi^{(3)} \bullet\bullet\bullet \mathbf{EEE} + \ldots \qquad (2.3)$$

p = the polarization vector (direction and intensity of the induced polarization). $\chi^{(1)}$, $\chi^{(2)}$, and $\chi^{(3)}$ are respectively the linear, second order nonlinear, and third order nonlinear polarization susceptibility tensors. Tensors are used to account for the variation of the linear or nonlinear polarization susceptibility with the direction of the applied electric field **E** and to describe the polarization induced in the ensemble of the macroscopic material. We see in equation (2.3) that for small electric fields of electromagnetic radiation (weak sources of light such as daylight or a desk lamp) the nonlinear polarizability (or hyperpolarizability) of materials is a very weak effect. Indeed, all the nonlinear polarization terms in equation (2.3) are dependent on powers of the electric field. If the electric field

of a source of light generates a force which rivals the coulombian forces between the electrons and the nuclei in the material on which the light is incident (such as the electric field from a laser source), the second and third order nonlinear polarization terms become significant and the polarization of the electrons oscillates anharmonically with the inducing electric field. This implies that the polarization of the electrons in the material will not vary linearly with the intensity of the incident light (as we can see from equation (2.3)). Also, the electrons in the material are subjected to an anharmonic acceleration. Thus, the electrons can experience different accelerations and reradiate the incident light at different frequencies. Second harmonic generation (SHG) is a second order nonlinear optical spectroscopy technique (it is described by the second term in equation (2.3)). A laser beam of frequency ω, may be reradiated (or reflected) at ω and 2ω. The light reradiated at 2ω is called the SHG signal. The SHG signal intensity is proportional to the square of the second order nonlinear polarization susceptibility tensor:

$$I_{SHG} \propto |\chi^{(2)}|^2 \qquad (2.4)$$

$\chi^{(2)}$ is dependent on the electronic structure of the material.

Second order nonlinear effects are not observed in centrosymmetric optical materials (material with inversion symmetry) such as glass, liquids, and gases. The reason for this is that the second order nonlinear polarization can occur symmetrically in these materials, thus cancelling out the effect ($\chi^{(2)}$ vanishes). Since our Au(111) single crystal substrate is centrosymmetric, the only region where $\chi^{(2)}$ will be non vanishing (where SHG will occur) is at the Au(111)/electrolyte interface, where the symmetry is broken. Thus, SHG is a surface/interface specific probe that can monitor the changes in

the electronic structure of the Au(111)/electrolyte interface when the potential of the electrode is changed [19,26]. Since we were not dealing with only the gold surface in our experiments, we rename $\chi^{(2)}$ as χ_{tot}. The C16 coated Au(111) in contact with an electrolyte solution produces an interface which may present different contributions from the different parts of the interface.

Experimental:

Our spectroelectrochemical cell was used for these experiments. Both the cell and the optical setup are described in Figure 2.3. The CaF_2 disc was used as the optical window mounted at the bottom of the cell. In these experiments, it was not necessary to press the Au(111) substrate against the optical window since the process of SHG occurs at the Au(111)/electrolyte interface and is not influenced by the amount of electrolyte that the laser radiation has to go through (since H_2O is transparent at 1064 nm and 532 nm). The Au(111) surface was brought to within 1 mm of the optical window. The source of radiation was an Active Passive, Mode-Locked, Q-switched, pulsed picosecond Nd:YAG laser [27] with a fundamental wavelength of 1064 nm. A picosecond laser was used in order to have more peak power in a shorter period of time. In this fashion, the second harmonic optical process was more efficient. Q-switching down to the picosecond timescale was accomplished with a saturable absorber. The saturable absorber was a dye called "Exciton Q-Switch-1" with a molecular weight of 763.33 g/mol. Q-switching is the act of modifying the resonance characteristics of the laser cavity. A population inversion in the Nd:YAG crystal is established while the laser cavity is not lasing the 1 μm light (the dye is absorbing). Then, when the dye gets saturated, it cannot absorb the intense radiation of the excited laser cavity and becomes transparent on the picosecond timescale. When this happens, the laser cavity lases and a picosecond burst of laser radiation can escape the laser cavity. The laser energy is thus concentrated in a smaller period of time. The optical setup for the SHG experiments is shown in Figure 2.6. The laser radiation, which comes

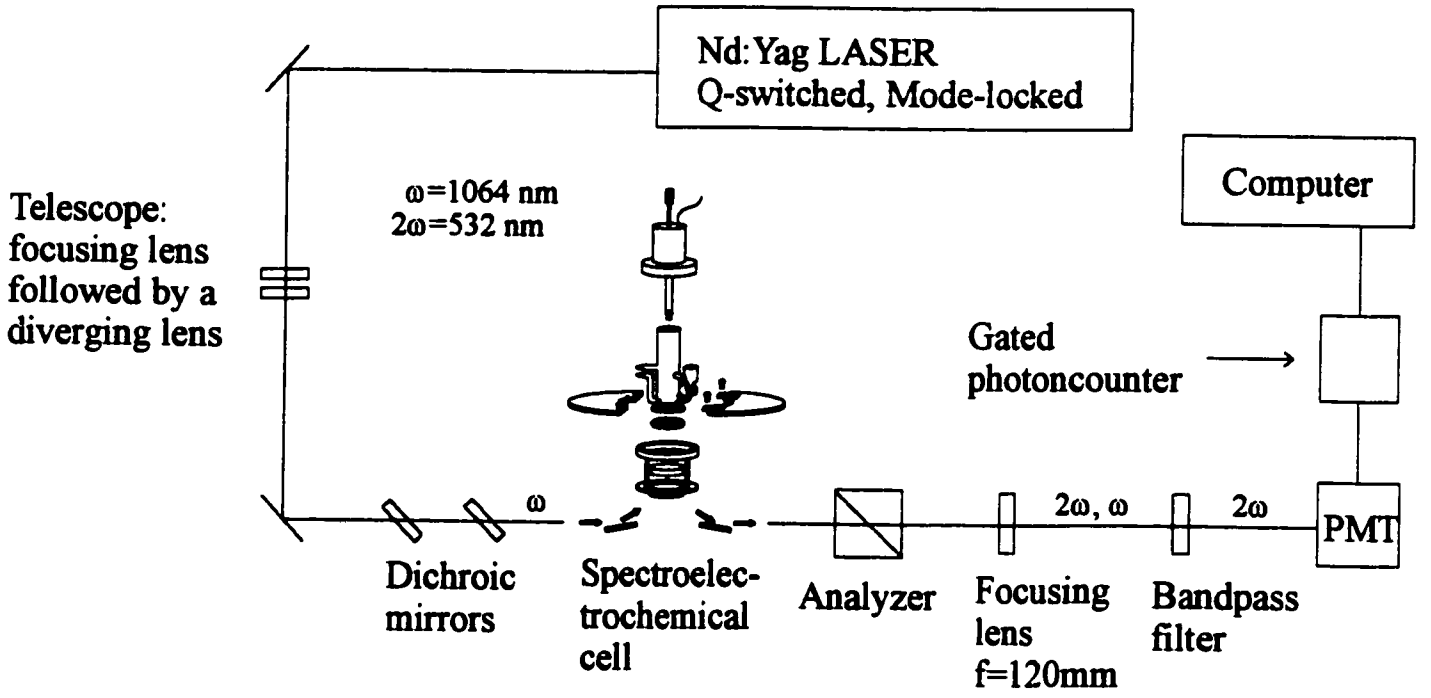

Figure 2.6: Optical setup for SHG spectroscopy.

out S-polarized from the laser, is directed through a telescope to focus it into a beam of around 1 mm in diameter. Then, the beam is directed through two dichroic mirrors which transmit at 1064 nm and reflect at 532 nm. This is done to screen out the 532 nm light that comes naturally from the laser due to second harmonic generation from the optical components. After this, the laser beam reaches the optical setup of the spectroelectrochemical cell. When the fundamental laser beam at 1064 nm hits the gold mirrors of the cell's optical bench, a SHG background signal is generated. To this background is added the SHG from the Au(111)/electrolyte interface. The light which is reflected from the Au(111) sample is directed through an analyzer to select either the S-polarized or the P-polarized radiation output of the Au(111) sample. Finally, the light from the Au(111) sample passes through a focusing lens with a 120 mm focal length and a bandpass filter allowing only the passage of 532 nm light. The signal coming through the bandpass filter is then detected by a photomultiplier tube (PMT) (Hamamatsu R4220P). The SHG photons were counted with a gated photoncounter (Stanford Sr 400). The photocounter's gate was triggered by the same signal that triggered the flash lamp. Because lasing occurs 150 ± 10 μs after the flash lamp triggering signal, the gate of the photoncounter was opened ~ 140 μs later for a period of 20 μs to count the SHG photons. Gating prevents pulses that are outside of the time interval we were interested in from being counted and it also improves the signal/noise ratio. Data acquisition from the photocounter was done with a computer via a GPIB interface and the Labview software for Windows (National Instrument Corporation). We found that the changes in the SHG signal intensity observed in our experiments were the largest when the laser output and the Au(111) sample output were S-polarized. The S-S polarization configuration enhances the detection of SHG from the adsorbate (C16 monolayers) [28]. This reinforces our arguments presented in Chapters 3 and 4, that the changes in the SHG are not only due to the interaction of our adsorbate with the substrate. They are also due to the presence of

a hyperpolarizable physisorbed state.

CHAPTER 3: In situ Vibrational Spectroscopy Results

We begin this chapter by introducing the electrochemical characteristics of a C16 monolayer chemisorbed on a Au(111) single crystal. This will provide a basis for all the spectroelectrochemical experiments that follow.

Introduction:

3.1 Electrochemical characterization of a C16 monolayer chemisorbed on a Au(111) single crystal:

Figure 3.1(a) depicts a typical cyclic voltammogram of a C16 monolayer chemisorbed on Au(111). This voltammogram is obtained as follows. A chemically coated (monolayer has been deposited chemically) Au(111) surface is brought in contact with the electrolyte (0.1 M KOH) while holding the potential at - 0.30 V. The potential is then scanned from - 0.30 V to - 1.25 V three times. We do this in order to get a cyclic voltammogram with repeatable features from cycle to cycle. Figure 3.1(a) represents a typical third cyclic voltammogram. On the negative going potential scan, we observe a reductive voltammetric wave composed of two peaks, A at - 1.13 ± 0.01 V and B at - 1.20 V ± 0.01 V. This voltammetric wave has been ascribed to a two-step reductive desorption of chemisorbed thiols [16,17,29]. After the reduction, a monolayer of physisorbed thiolates is formed because of the insolubility of C16 in 0.1 M KOH. On the subsequent positive going potential scan, we observe an oxidative voltammetric wave composed of two peaks, B' at - 0.99 ± 0.01 V and A' at - 0.93 ± 0.01 V. This voltammetric wave has been ascribed to a two-step oxidative redeposition

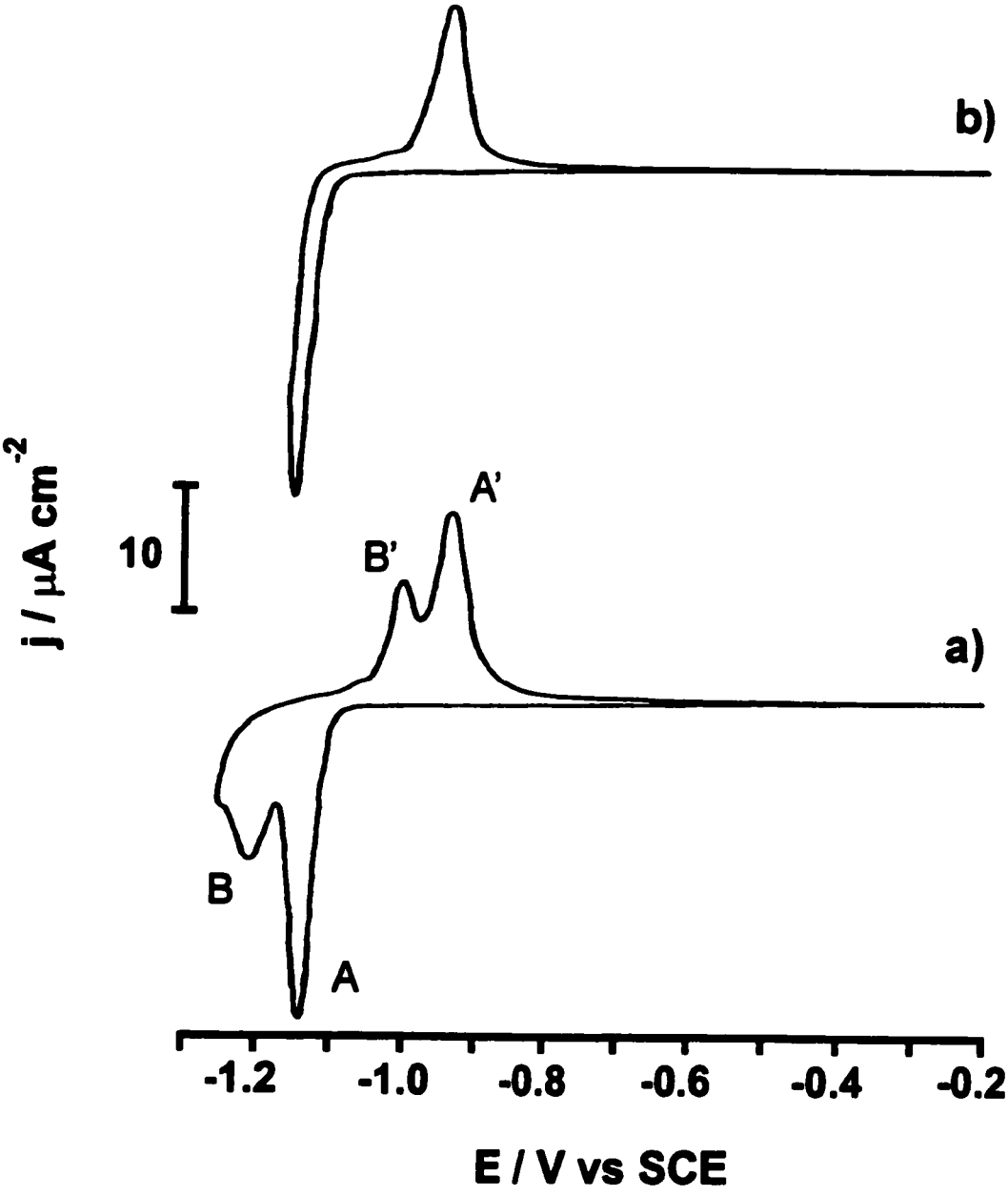

Figure 3.1: Cyclic voltammograms of a Au(111) electrode covered with a monolayer of C16 recorded: (a) between - 0.20 V and - 1.25 V; (b) between - 0.20 V and - 1.16 V.

of physisorbed thiolates [16,17,29]. The charge integration for the reductive voltammetric wave is equal to that of the oxidative voltammetric wave. These integrations yield a value of 85 ± 5 $\mu C\ cm^{-2}$ which is 10-15 % lower than the integration obtained for the first cyclic voltammogram. Consequently some adsorbate molecules are lost in the first cycle. Window opening experiments have shown that peaks A and B of the reductive voltammetric wave relate to peaks A' and B' of the oxidative voltammetric wave respectively [16]. Indeed, if we carry out a cyclic voltammetry experiment on the C16/Au(111) system where we scan the potential between - 0.30 V and - 1.16 V (potential just before peak B), we only see peaks A and A' in the cyclic voltammogram. Such an experiment is shown in Figure 3.1(b). It is important to note that the symmetrical shape of peak A' and its width at half height of ~ 60 mV in Figure 3.1(b) are characteristic of an oxidation process of one electron per adsorbate.

A precise determination of the charge corresponding to the current peaks A and B and A' and B' would provide us with the charge distribution between each step of the reduction and the oxidation processes. This could then help us elaborate a mechanism to explain the two steps. Unfortunately, the overlap of the current peaks for the reduction and oxidation processes disallows this. Nevertheless, we may estimate the charge distribution between the two steps for the reduction and the oxidation processes to give us a rough idea. For the oxidation process, we estimated the charge distribution between the two steps by measuring the amount of oxidative charge redeposited when the peak B' disappears from the positive going potential scan recorded after holding the potential at - 1.01 V for 3 minutes. We find that peak B' represents 36 ± 7 % of the total oxidative charge. This means that 1/3 (25 - 30 $\mu C\ cm^{-2}$) of the total oxidative charge is associated with peak B' whereas 2/3 (55 - 60 $\mu C\ cm^{-2}$) are associated with peak A'. For the reduction process, we recorded a cyclic

voltammogram at a very slow potential scan rate (0.5 mV s^{-1}) which provided a better separation of the peaks A and B. Thus we determined that 2/3 of the total reductive charge are associated with peak A whereas 1/3 are associated with peak B. These estimates suggest once again that peaks B and B' and A and A' are related. From these estimates we conclude that the reduction/oxidation of 80 - 85 % of a monolayer can be accounted for by peaks A and A' whereas 15 - 20 % can be accounted for by peaks B and B'.

Results and discussion:

3.2 Ex situ FTIR spectroscopy of a C16 monolayer on Au(111):

The experiments of this section were carried out in order to determine if an electrodeposited monolayer is spectroscopically the same as a chemically deposited monolayer. This was prompted by the electrochemical changes observed between a chemically deposited monolayer and an electrodeposited monolayer in the previous section. Indeed, we may recall that 10-15 % of the charge measured for the reductive desorption of a chemically deposited monolayer in the first cyclic voltammogram is lost in the third cyclic voltammogram (corresponding to an electrodeposited monolayer). This is accompanied by changes in the features (intensity and resolution of the peaks A and B and intensities of peaks B' and A') of the first two cyclic voltammograms. These features stabilize after two voltammograms.

The vibrational spectra of the C-H stretching region for the chemically and electrochemically deposited monolayers are shown in Figure 3.2. The IR spectrum of a chemically deposited C16

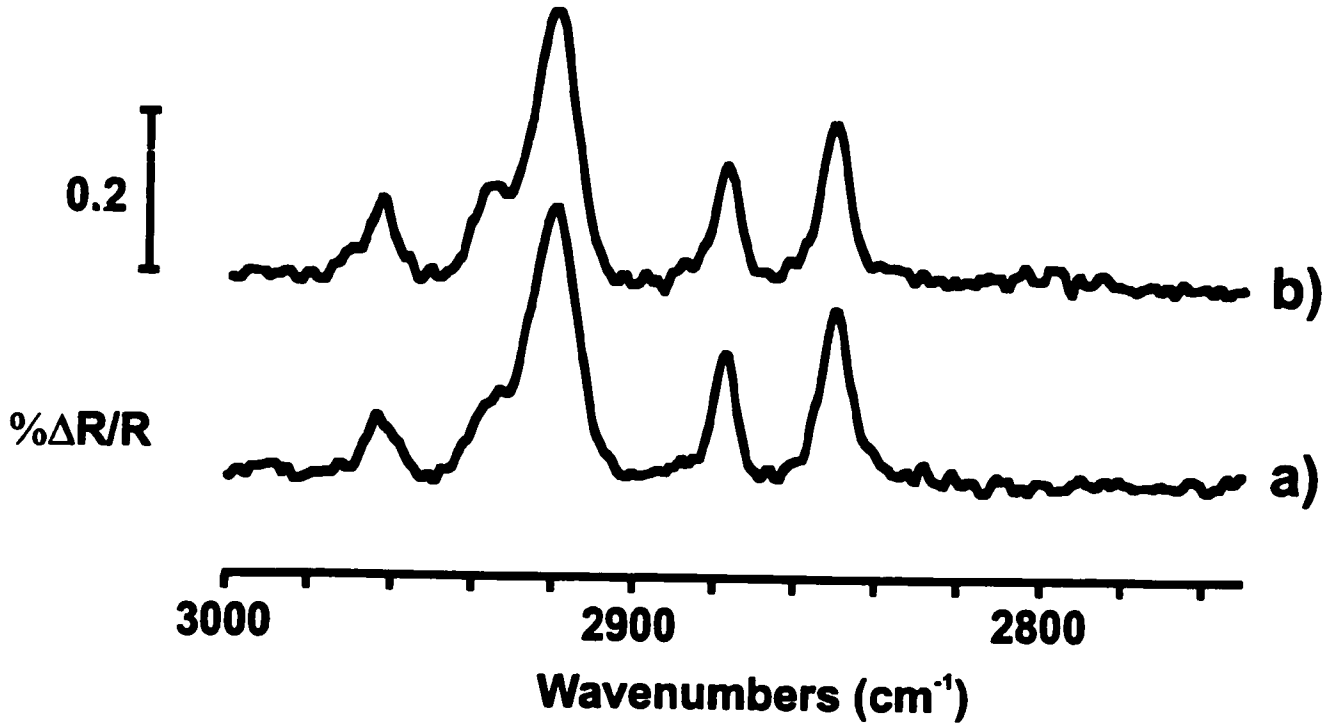

Figure 3.2: Differential reflectance spectra of (a) a chemically deposited monolayer of C16 on Au(111); (b) the same monolayer after being reductively desorbed and oxidatively redeposited twice.

monolayer (Figure 3.2(a)) exhibits 5 C-H stretching bands and is identical to previously reported spectra [7,30]. The bands at 2964, 2937, and 2878 cm^{-1} correspond to the in-plane asymmetric CH_3 stretch, the first and the second Fermi resonances respectively. The Fermi resonances result from the coupling of the symmetric CH_3 stretching and bending modes (see Figure 3.3 for a pictorial interpretation). The bands at 2919 and 2851 cm^{-1} correspond to the CH_2 symmetric and asymmetric stretching modes respectively. The wavenumbers for the CH_2 symmetric and asymmetric stretching modes are characteristic of an all-trans configuration of the alkane chain of C16, indicating that the C16 monolayer is well ordered. We see that the spectrum of an electrodeposited monolayer in Figure 3.2(b) is identical to that of a chemically deposited monolayer. The spectrum in Figure 3.2(b) was obtained as follows. A chemically coated Au(111) surface was brought in contact with 0.1 M KOH at - 0.30 V. The potential was then scanned from - 0.3 V to - 1.30 V two times. The Au(111) electrode resulting from this treatment was rinsed with Milli-Q water and transferred into the FTIR spectrometer. The spectrum was acquired. This experiment shows that the chemically and electrochemically deposited monolayers have the same average orientation of their alkane chains. The 10-15 % loss of charge between the first and third cyclic voltammograms does not influence the intensity of the bands in Figure 3.2(b). Most probably, this 10-15 % loss is due to thiols adsorbed on the edge of the electrode which do not contribute to the IR spectrum. Hence, it is possible to electrodeposit a C16 monolayer onto Au(111) in a few seconds and obtain the same average orientation of the alkane chains as for a chemically deposited monolayer.

3.3 In situ FTIR spectroscopy of a C16 monolayer on Au(111):

This section provides some insight into the evolution of the orientation of the C16 alkane chains

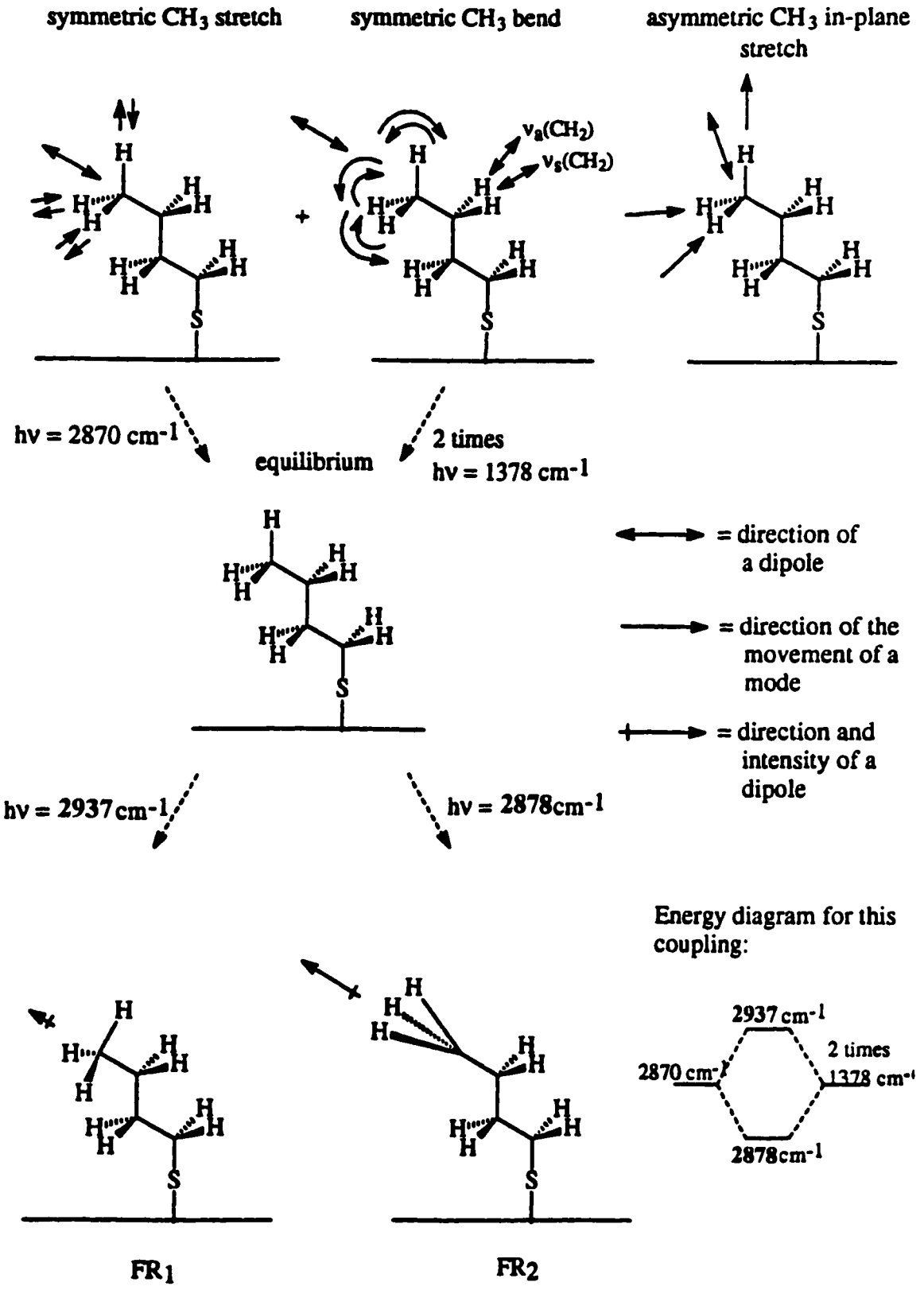

Figure 3.3: The origin of the Fermi resonances.

with respect to the Au(111) surface when the substrate is subjected to different potentials. In situ vibrational spectroscopy (SNIFTIRS) was used to accomplish this. We will look at the reductive desorption and the oxidative redeposition of a C16 monolayer on Au(111) first. Secondly, we will examine the changes in the orientation of the C16 alkane chains when the substrate is subjected to potentials going into the different peaks B' and A' and A and B of the oxidative redeposition and the reductive desorption respectively.

A SNIFTIRS spectrum is obtained by taking the difference of two spectra measured at fixed potentials. Thus SNIFTIRS measurements are done in equilibrium conditions. Each of the spectra acquired at fixed potentials requires 200 scans at a resolution of 2 cm^{-1} to obtain a good signal to noise ratio. In this fashion, every spectrum takes ~ 3 minutes to acquire for a total of ~ 6 minutes of acquisition time per SNIFTIRS spectrum. This corresponds to spending ~ 3 minutes in the physisorbed state of a C16 monolayer in each SNIFTIRS spectrum. Since the cyclic voltammograms of C16 on Au(111) are acquired under non-equilibirum conditions (potential scanned at 20 mV s^{-1}), we had to verify the stability of the physisorbed C16 monolayer for 3 minutes in order to verify that the SNIFTIRS spectra are related to the current peaks in the cyclic voltammogram of Figure 3.1(a). We carried out this verification by reducing a C16 monolayer via a negative going potential scan from - 0.30 V to - 1.25 V, and then holding the potential at - 1.25 V for 3 minutes. Afterwards, the physisorbed monolayer was oxidatively redeposited by scanning the potential back to - 0.30 V. The voltammogram that resulted from this positive-going scan is shown in Figure 3.4. We notice that the relative intensities of the current peaks B' and A' and the potentials at which they appear are the same as those observed in a continuous voltammogram (Figure 3.1(a)).

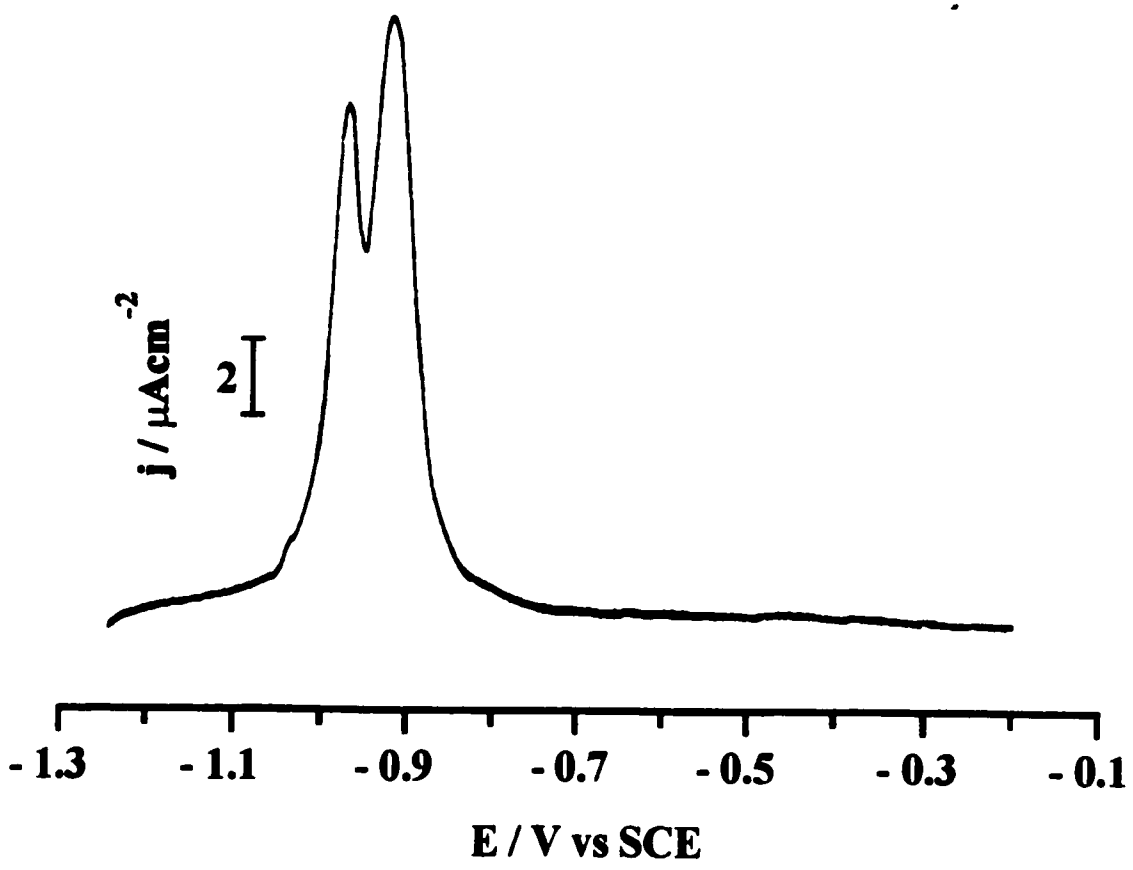

Figure 3.4: Voltammogram recorded after scanning the potential of a Au(111) electrode covered with a monolayer of C16 from - 0.30 V to - 1.25 V and holding the potential at - 1.25 V for 3 minutes and then scanning the potential to - 0.30 V.

The SNIFTIRS spectra in Figures 3.5(a) and 3.5(b) correspond to the reductive desorption and the oxidative redeposition of C16 on Au(111) respectively. For the reductive desorption, the reference spectrum was taken at - 0.30 V (potential at which the C16 monolayer is chemisorbed) and the potential was jumped from - 0.30 V to - 1.20 V. For the oxidative redeposition, the reference potential was at - 1.20 V (potential at which the C16 monolayer is physisorbed) and the potential was jumped from - 1.20 V to - 0.30 V. When the C16 monolayer is reduced, we observe two negative peaks at 2926 and 2855 cm^{-1}. These two peaks correspond to an increase of the intensities of the CH_2 asymmetric and symmetric stretching modes with the reductive potential jump. There is a shift to higher wavenumbers of these vibrational modes compared with spectra taken in air (Figure 3.2). This is an indication that a monolayer in contact with an aqueous electrolyte becomes disordered [22,31,32]. However, it is believed that this disorder is present mainly at the thiol/liquid interface [31,32]. The idea of localized disorder at this thiol/liquid interface supports the fact that the CH_3 stretching modes are absent in the spectra of Figures 3.5(a) and 3.5(b). Disordered CH_3 groups would exhibit weak and broad C-H stretching bands in the chemisorbed and the physisorbed states. Variations of the intensity of the CH_3 stretching bands between the chemisorbed and physisorbed states would be undetectable. The decrease in the percentage reflectance (% $\Delta R/R$) observed at 2926 and 2855 cm^{-1} indicates that more absorption of the IR radiation occurs at these frequencies when a C16 monolayer goes to a physisorbed state. According to the IR surface selection rules [33], this means that the transition dipoles (TD, i.e. electric dipole variation) of the CH_2 stretching modes become on average more perpendicular to the surface. If we assume an all-trans configuration for the alkane chains, given that the TD's of the CH_2 stretching modes are perpendicular to the molecular axis of an all-trans alkane chain, we can deduce that the C16 molecules, in going from a chemisorbed state to a physisorbed state, become more parallel to the surface (on average). This assumption is

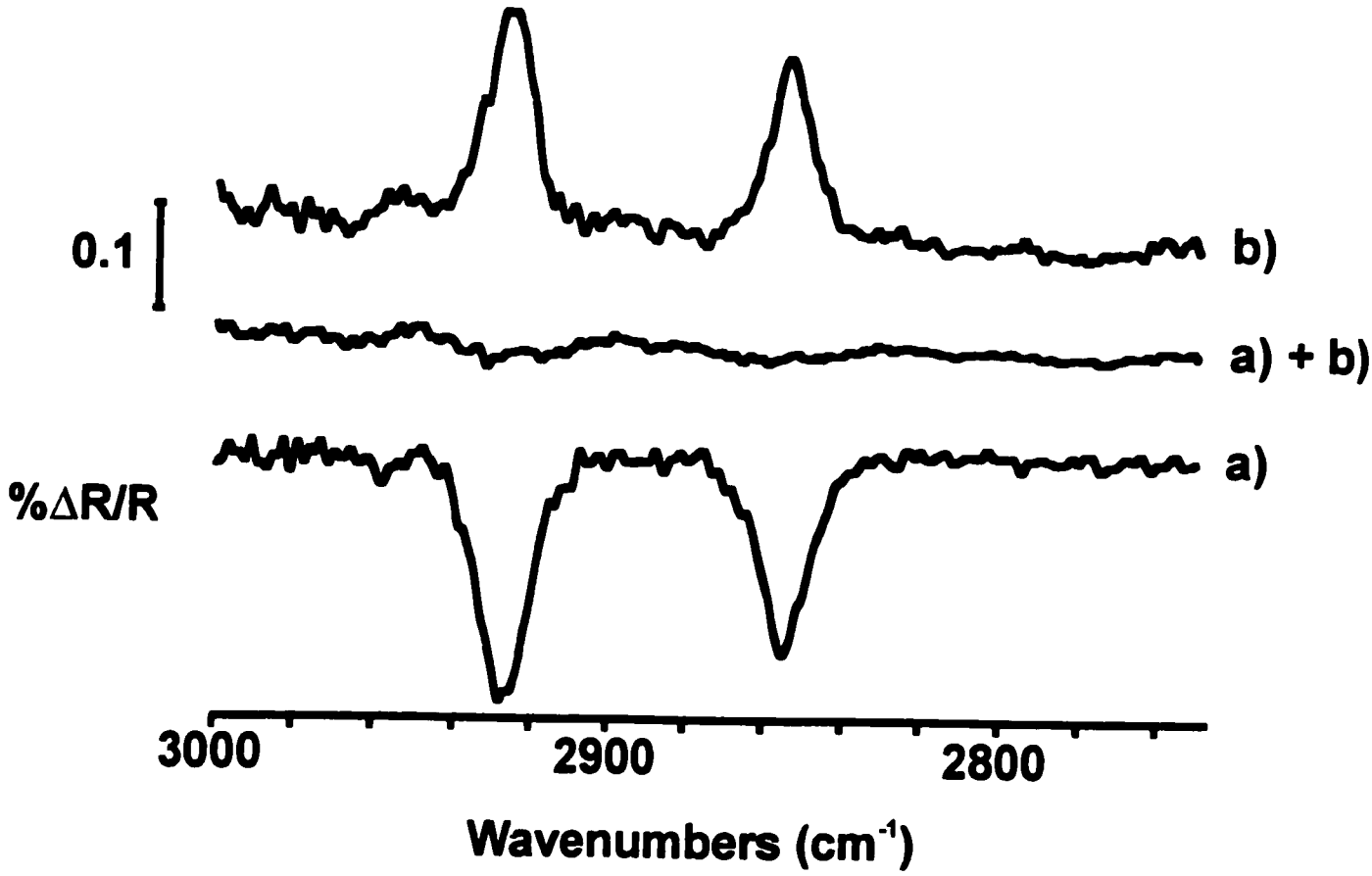

Figure 3.5: SNIFTIRS spectra of a monolayer of C16 chemisorbed on Au(111) resulting from (a) a potential step from - 0.30 V to - 1.20 V and (b) a potential step from - 1.20 V to - 0.30 V; the sum of spectra (a) and (b) is presented as a) + b). Each spectrum is an average of five different sets of 200 spectra recorded at a resolution of 2 cm^{-1}.

considered appropriate based on the fact that an electrodeposited monolayer exhibits an IR spectrum characteristic of an all-trans configuration of the alkane chains of C16. Indeed, this suggests that in going from a chemisorbed to a physisorbed state of a C16 monolayer, no significant amount of gauche defects are created. When the physisorbed C16 monolayer gets electrodeposited back onto the Au (111) surface, we observe two positive peaks at 2926 and 2855 cm^{-1}. These two peaks correspond to the variation of the intensities of the CH_2 asymmetric and symmetric stretching modes with the oxidative potential jump.The increase in the percentage reflectance (% $\Delta R/R$) observed at 2926 and 2855 cm^{-1} indicates that less absorption of the IR radiation occurs at these frequencies when a C16 monolayer returns to a chemisorbed state. Again, if we assume an all-trans configuration of the alkane chains, according to the surface selection rules, we may deduce that the C16 molecules, in going from a physisorbed state to a chemisorbed state, become more perpendicular to the surface (on average).

If we add the spectra of Figures 3.5 (a) and (b), we get an almost perfect cancellation of the CH_2 bands at 2926 and 2855 cm^{-1}. Consequently, the changes in the orientation of the alkane chains of a C16 monolayer observed throughout a reductive desorption/oxidative redeposition cycle are reversible. This is also concordant with the fact that an electrodeposited monolayer and a chemisorbed monolayer are spectroscopically identical (same average orientation of the alkane chains). It is important to mention at this point that when the same in situ experiments are carried out in S-polarized light, we observe no peaks in the SNIFTIRS spectra. This undoubtedly indicates that the C16 molecules do not leave the surface when they get reduced. They remain physisorbed.

We can explain the reorientation of the C16 molecules that occurs throughout a reductive

desorption/oxidative redeposition cycle via a balance of electrostatic forces. When a Au(111) substrate is covered by a full monolayer of C16, the distance that separates each C16 molecule from the others is only 5 Å [34]. Upon reducing the C16 monolayer, the negatively charged sulfur head groups formed will obviously feel strong repulsive electrostatic forces from one another at this short distance. In order to get the least repulsion, the negative sulfur head groups will move to greater distances from each other, thus causing a reorientation of the C16 alkane chains. It is understandable that a positive going potential jump or scan will cause the negative sulfur head groups to come closer to the Au(111) surface via attractive forces, thus reorienting the physisorbed thiolates. It is important to mention that it would not be possible to observe these reorientations of the alkane chains if it were not for the low solubility of C16 thiolates in an aqueous electrolyte. This point will be addressed in the experiments presented below.

The experiments that follow were carried out to determine if there is a relationship between the current peaks of the cyclic voltammogram in Figure 3.1(a) and the changes in the SNIFTIRS spectra. We first look at the oxidative redeposition of physisorbed C16 thiolates onto the Au(111) substrate. The intensity of the band at 2926 cm^{-1} of the SNIFTIRS spectrum was measured for a series of potential steps from - 1.20 V to potentials between - 1.10 V and - 0.85 V. The spectrum taken at - 1.20 V (corresponding to a monolayer of physisorbed C16 thiolates) was the reference for each potential step. We normalized the measured intensities by dividing them with the intensity of the band at 2926 cm^{-1} in a SNIFTIRS spectrum obtained for a potential step from - 1.20 V to - 0.30 V (corresponding to the complete electrodeposition of a monolayer of physisorbed C16 thiolates). The normalized IR intensities, denoted as I_{Norm}^{ox}, versus potential are graphed in Figure 3.6. Each normalized IR intensity is an average of three measurements done on different monolayers. I_{Norm}^{ox}

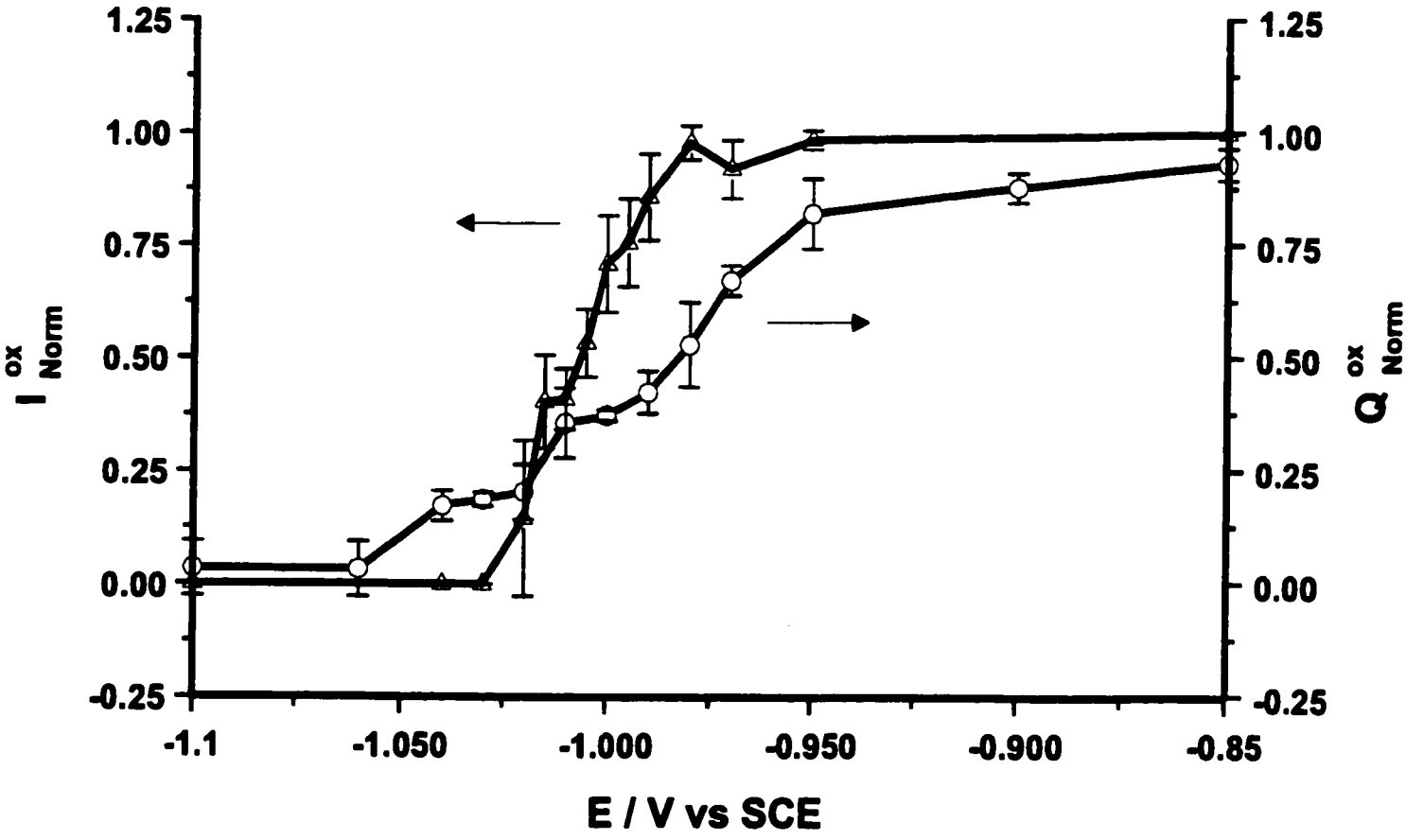

Figure 3.6: Normalized intensities of the band at 2926 cm^{-1}, I_{Norm}^{ox}, and the normalized oxidative charges, Q_{Norm}^{ox}, measured after potential steps from - 1.20 V to potentials between - 1.10 V and - 0.85 V. Each data point is an average of three measurements. Each measurement is an average of 200 spectra recorded at a resolution of 2 cm^{-1}. See the text for more details.

represents the % amount of IR intensity change that occurs as we go through the oxidative peaks B' and A' in small potential increments. The Q_{Norm}^{ox} values in Figure 3.6 were determined as follows. A C16 monolayer was reduced by scanning the potential of the Au(111) substrate from - 0.30 V to - 1.30 V. Upon the positive going potential scan, the potential was held at E_{hold}^{ox} (E_{hold}^{ox} = potentials between - 1.10 V and - 0.85 V) for 3 minutes. Then the potential was scanned positively from E_{hold}^{ox} to - 0.30 V. The voltammogram resulting from this positive going potential scan was integrated to yield the oxidative charge Q^{ox}. Immediately after acquiring the voltammogram from E_{hold}^{ox} to - 0.30 V, we continued the potential scanning to record another voltammogram of the oxidative redeposition from - 1.30 V to - 0.30 V. This voltammogam was integrated from - 1.30 V to - 0.30 V to provide the total oxidative charge, Q_{total}^{ox}. $Q_{Norm}^{ox} = (Q_{total}^{ox} - Q^{ox})/Q_{total}^{ox}$. Q_{Norm}^{ox} represents the fraction of the oxidative charge deposited for each of the I_{Norm}^{ox} measured. The Q_{Norm}^{ox} values in Figure 3.6 are averages of three measurements done on different monolayers.

Figure 3.6 clearly demonstrates that the IR changes happen on a shorter potential range than the deposition of oxidative charge. I_{Norm}^{ox} increases from 0 % to 100 % over a 50 mV range (from - 1.03 V to - 0.98 V), whereas Q_{Norm}^{ox} increases from 0 % to 100 % over a 260 mV range (from - 1.06 V to - 0.80 V). Two plateaux present themselves throughout the variation of Q_{Norm}^{ox}. Q_{Norm}^{ox} is constant and equal to 20 ± 2 % in the first plateau which ranges between - 1.04 V and - 1.02 V. Q_{Norm}^{ox} is constant and equal to 40 ± 4 % in the second plateau which ranges between - 1.01 V and - 0.99 V. Q_{Norm}^{ox} increases smoothly after these plateaux. When we carried out the cyclic voltammetry experiments to determine the Q^{ox} values in the previous paragraph, we noticed that the current peak B' disappeared for potential holds at E_{hold}^{ox} values more positive than - 1.02 V. Based on this observation, we may ascribe most of the oxidative charge up to the second plateau to the

(disappearance of) current peak B'. We believe that the first plateau is related to a much smaller peak which shoulders at the base and on the more negative side of peak B' (see Figures 3.1(a) and 3.4). Since most of the IR intensity change happens in the range of the second plateau, we ascribe it to the disappearance of peak B'. The remaining charge after the second plateau (60 %) is ascribed mostly with peak A'. Indeed, the potential range after the second plateau corresponds closely to the potential of peak A' in the cyclic voltammogram of Figure 3.1(a).

Experiments were carried out in a similar fashion for the reductive desorption of C16 on Au(111). The SNIFTIRS spectra were measured for a series of potential steps from - 0.30 V to potentials between - 1.04 V and - 1.20 V. The spectrum taken at - 0.30 V (corresponding to a chemisorbed monolayer of C16) was the reference for each potential step. We normalized the intensities measured at 2926 cm^{-1} by dividing them with the intensity of the same band in a SNIFTIRS spectrum obtained for a potential step from - 0.30 V to - 1.20 V (corresponding to the complete reductive desorption of a chemisorbed C16 monolayer). The normalized IR intensities, denoted as I_{Norm}^{red}, versus potential are graphed in Figure 3.7. I_{Norm}^{red} represents the percent amount of IR intensity change that occurs as we go through the reductive peaks A and B in small potential increments. The Q_{Norm}^{red} values in Figure 3.7 were determined as follows. We scanned the potential of our C16/Au(111) system from - 0.30 V to a potential E_{hold}^{red} (E_{hold}^{red} = values between - 1.04 V and - 1.20 V). On reaching E_{hold}^{red}, the potential was held there for 3 minutes, after which we recorded the oxidative redeposition voltammogram. The negative of the integration of this voltammogram provided us with the reductive current, Q^{red}. This is appropriate since the amount of the reductive charge deposited at E_{hold}^{red} must be equal to the oxidative charge deposited in the subsequent scan from E_{hold}^{red} to - 0.30 V. Following the determination of Q^{red}, a cyclic voltammogram was recorded from - 0.30 V to - 1.30 V. The

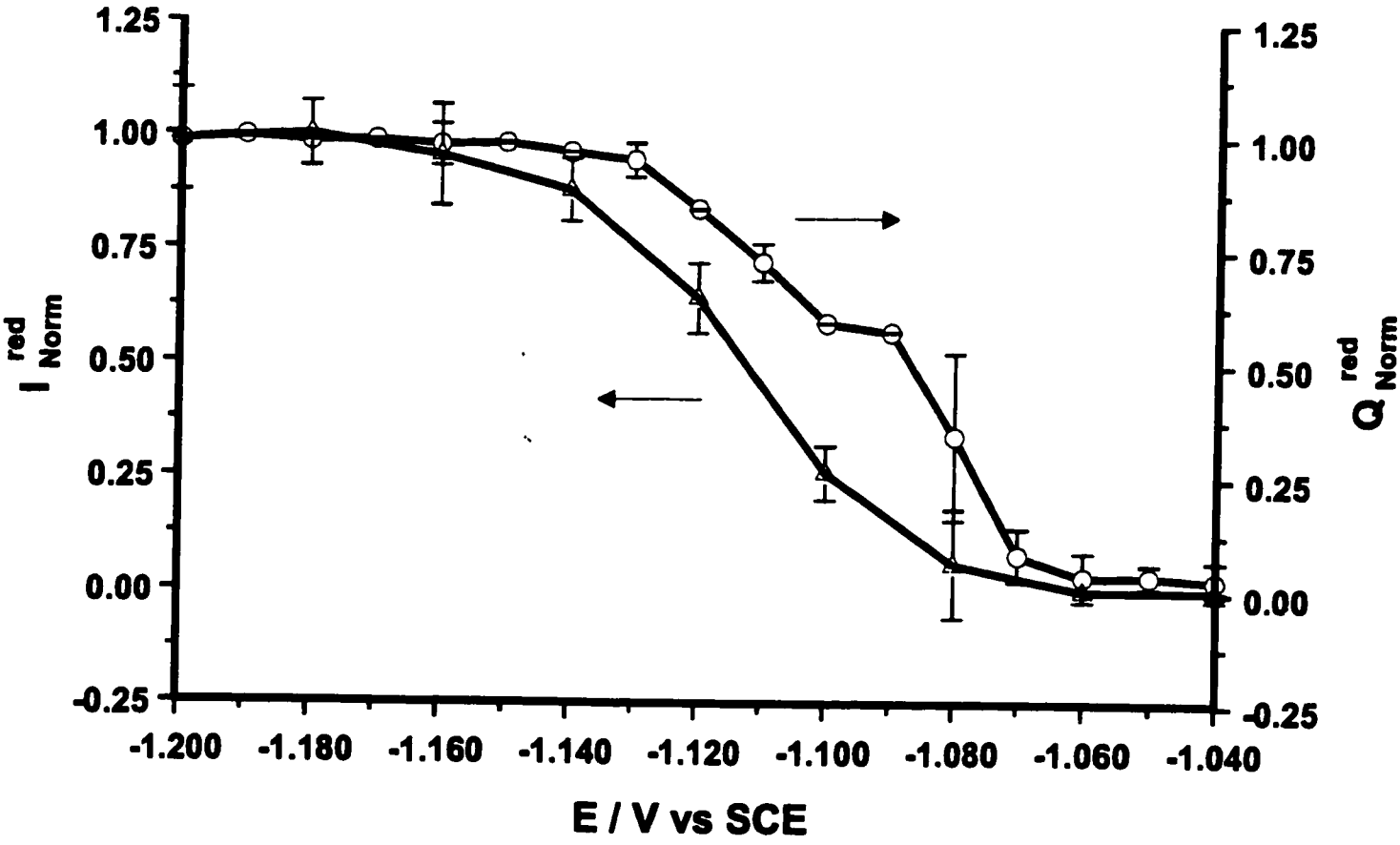

Figure 3.7: Normalized intensities of the band at 2926 cm^{-1}, I_{Norm}^{red}, and the normalized reductive charges, Q_{Norm}^{red}, measured after potential steps from - 0.30 V to potentials between - 1.04 V and - 1.20 V. Each data point is an average of three measurements. Each measurement is an average of 200 spectra recorded at a resolution of 2 cm^{-1}. See the text for more details.

integration of this voltammogram from - 0.30 V to - 1.30 V provided us with the reductive charge for the total reductive desorption of a C16 monolayer, Q_{total}^{red}. The normalized reductive charge $Q_{Norm}^{red} = Q^{red}/Q_{total}^{red}$. Q_{Norm}^{red} represents the fraction of reductive charge deposited for each of the I_{Norm}^{red} measurements. The I_{Norm}^{red} and Q_{Norm}^{red} values in Figure 3.7 are averages of three measurements done on different monolayers.

Figure 3.7 shows that the changes in I_{Norm}^{red} and Q_{Norm}^{red} vary over the same potential range. I_{Norm}^{red} varies from 0 % at - 1.08 V to 100 % at - 1.16 V. Q_{Norm}^{red} goes from 0 % to 100 % between - 1.06 V and - 1.13 V. This differs from what we have seen for the oxidative redeposition. However, we notice the differences in the way I_{Norm}^{red} and Q_{Norm}^{red} vary with potential. We see that at a potential of - 1.08 V, there is a large standard deviation of ± 18 % for the value of Q_{Norm}^{red}. This is indicative of a variable onset of the reduction of C16 from one monolayer to another. Also, while I_{Norm}^{red} varies smoothly throughout the potential range corresponding to the current peaks A and B, Q_{Norm}^{red} presents a plateau between - 1.09 V and - 1.10 V which levels at 57 ± 1 %. This reproducible plateau occurs within a small potential range that is just at the onset of the current peak A. In this manner, we ascribe the charge up to this plateau to the current peak A. The remaining charge, 43 %, is associated mostly with peak B. The value of I_{Norm}^{red} corresponding to the plateau of Q_{Norm}^{red} is only 25 ± 5 %. This means that most of the IR intensity changes occur in a potential range after the Q_{Norm}^{red} plateau. Thus the IR intensity changes are mostly ascribed to peak B.

The results of Figures 3.6 and 3.7 provide strong evidence that the reductive desorption and the oxidative redeposition of a C16 monolayer occur in two consecutive steps. One step involves the reduction/oxidation of most of the C16 molecules (60 % of the charge here). This step corresponds

to peaks A and A'. We observe small changes in the orientation of the C16 alkane chains for this step (IR intensity changes are small). The other step involves a significant change in the orientation of the C16 alkane chains (IR intensity changes are large). This step corresponds to peaks B and B'. The charge associated with this step is smaller (40 %).

The charge distribution between peaks B-B' (40 %) and A-A' (60 %) corresponds closely to the charge distribution estimated from a model used previously to determine the surface concentration of thiols from the reductive charge obtained in a cyclic voltammogram like the one in Figure 3.1(a) [18]. This model consists of a faradaic and a capacitive component. The faradaic component corresponds to the electron transfer from the electrode to the chemisorbed thiols. This component constitutes 70 % of the total reductive charge. The capacitive component is associated with the formation of a double layer (an arrangement of charges next to the surface of an electrode which counterbalances the charges at the surface of the electrode) when the thiols of a chemisorbed monolayer are reductively desorbed from the electrode surface. This component accounts for 30 % of the total reductive charge. When 70 % (69-71 $\mu C\ cm^{-2}$) of the total reductive charge obtained previously for C16 [18] was converted to a thiol coverage, assuming a one-electron per thiol process, the coverage was found to be $7.2 * 10^{-10} \pm 10$ % mol cm^{-2}. The full monolayer coverage of thiols (determined by calculating the number of thiols per unit area in the highest packing density on Au(111), i.e. 5 Å between each thiol, each thiol sitting in a three fold site), $7.6 * 10^{-10}$ mol cm^{-2}, was identical to the coverage obtained from this calculation. The percentage of the total reductive/oxidative charge associated with peaks A and A' (60 % or 55-60 $\mu C\ cm^{-2}$) is similar to the estimated fraction of the total reductive charge associated with the faradaic component. Consequently, we also observe this similarity between the percentage of the total reductive/oxidative

charge associated with peaks B and B' (40 % or 25-30 $\mu C\ cm^{-2}$) and the estimated fraction of the total reductive charge associated with the capacitive component. These comparisons suggest that the reductive desorption of a chemisorbed C16 monolayer proceeds via a faradaic step (peak A) followed by a capacitive step (peak B). The oxidative redeposition is simply the reverse of the reductive desorption. The capacitive step (peak B') precedes the faradaic step (peak A').

3.4 A new mechanism for the reductive desorption and the oxidative redeposition of low-solubility thiols:

The results that we have presented above disagree with the two models suggested in the literature to explain the origin of the two peaks in the reductive and oxidative voltammetric waves of C16 on Au(111). One model suggests that there are two domains with different packing densities [16,17]. In this model the peaks A and A' correspond to a low density domain whereas the peaks B and B' are related to the formation of a high density domain. In order for this model to fit with our results, the reduction of the low density domain (peak A) should cause little change in the orientation of the alkane chains whereas the high density domain should cause significant changes in the orientation of the alkane chains. Given that the surface coverage of thiols is high on Au(111), the difference between the densities of the two domains cannot be that great. Thus, the Coulombic repulsions between the thiolates will be as important in the low and high density domains. This means that the IR intensity changes should follow the changes of the charge fairly closely in this model. This is contrary to what we have observed in our results. The other model suggests the presence of two different adsorption sites for thiols on Au(111). This model is supported by ab initio calculations [35] that predict the presence of two stable adsorption sites, an on-top site and a three-fold site differing

by ~ 2 kcal mol^{-1}. As mentioned in the introduction, the existence of a second adsorption site was motivated by the greater chain-chain interactions for thiols with alkane chains containing more than 12 carbons. In this model, we expect that the reductive desorption of thiols from either of the two sites will cause changes in the orientation of the alkane chains. Thus, this model also predicts that the IR intensity changes should follow the changes in the charge. Once more, this is contrary to what we have observed in our results. It is important to mention that no evidence of the presence of two adsorption sites was found from XPS measurements on a C16 covered Au(111) substrate [16].

The two models presented in the previous paragraph do not take into account the large overpotentials required to reductively desorb thiols with long alkane chains. Indeed, these large overpotentials (C16 reductively desorbs at a potential 300 mV more negative than that for butanethiol), which are caused by the better charge screening and the very low solubilities of thiols with long alkane chains [16-18,29], have the effect of making the reduction of chemisorbed thiols much faster [36]. In this respect, models that explain the presence of two current peaks in the reduction and oxidation processes of low solubility thiols via two types of thiols with slightly different energies of reduction (as is the case for the two models disputed in the previous paragraph) are not valid. Indeed, two types of thiols with slightly different energies of reduction are expected to reductively desorb at similar rates. Therefore, the reduction process should not give rise to well-separated current peaks.

On the contrary, our results suggest a mechanism where all of the thiols reductively desorb or oxidatively redeposit in two consecutive steps. We suggest the following mechanism. The starting point is a chemisorbed monolayer of C16 on Au(111) in a 0.1 M KOH electrolyte at a potential of

- 0.30 V (Figure 3.8(a)). An all-trans configuration is assumed for the alkane chains. When we scan the potential from - 0.30 V up to - 1.06 V, we observe no faradaic current and no IR intensity changes. Hence the state represented by Figure 3.8(a) holds from - 0.30 V to - 1.06 V. At - 1.09 V the chemisorbed thiols get reduced via a one-electron per molecule process. This reduction step is associated with peak A and corresponds to the reduction of an almost complete monolayer C16 (80-85 %; see section 3.1). A slight change in the orientation of the alkane chains accompanies the current peak A (I_{Norm}^{red} = 25 % in the potential range associated with peak A). However, the majority of the reduced thiols maintain their original orientation, as depicted in Figure 3.8(b). Thus we have a lamellar type arrangement of physisorbed thiolates. Current peak A corresponds to going from the state of Figure 3.8(a) to the state of Figure 3.8(b). As we go to potentials more negative than - 1.10 V, the negative Au(111) surface repels the lamellar type arrangement of physisorbed thiolates. The formation of micelles of thiolates follows since the negative sulfur head groups repel themselves (Figure 3.8(c)). From our results, we cannot deduce the shape of the micelles formed. However, spherical micelles and hemi-micelles are two possibilities which are compatible with our results. Indeed, the alkane chains of aliphatic compounds forming micelles has been shown to be mainly all-trans [37]. In this respect, the formation of spherical micelles or hemi-micelles will increase the average number of alkane chains which are parallel to the Au(111) surface. The average number of CH_2 transition dipoles perpendicular to the Au(111) surface will thus be greater. Our SNIFTIRS results indicate an increase in the average number of CH_2 transition dipoles in going from a chemisorbed monolayer to a physisorbed monolayer. When the physisorbed micelles of thiolates are formed, a large portion of the Au(111) surface becomes unblocked. This allows the formation of an electrical double layer at the negatively charged unblocked Au(111) surface. The negative capacitive current caused by the formation of this double layer is associated with current peak B. Current peak

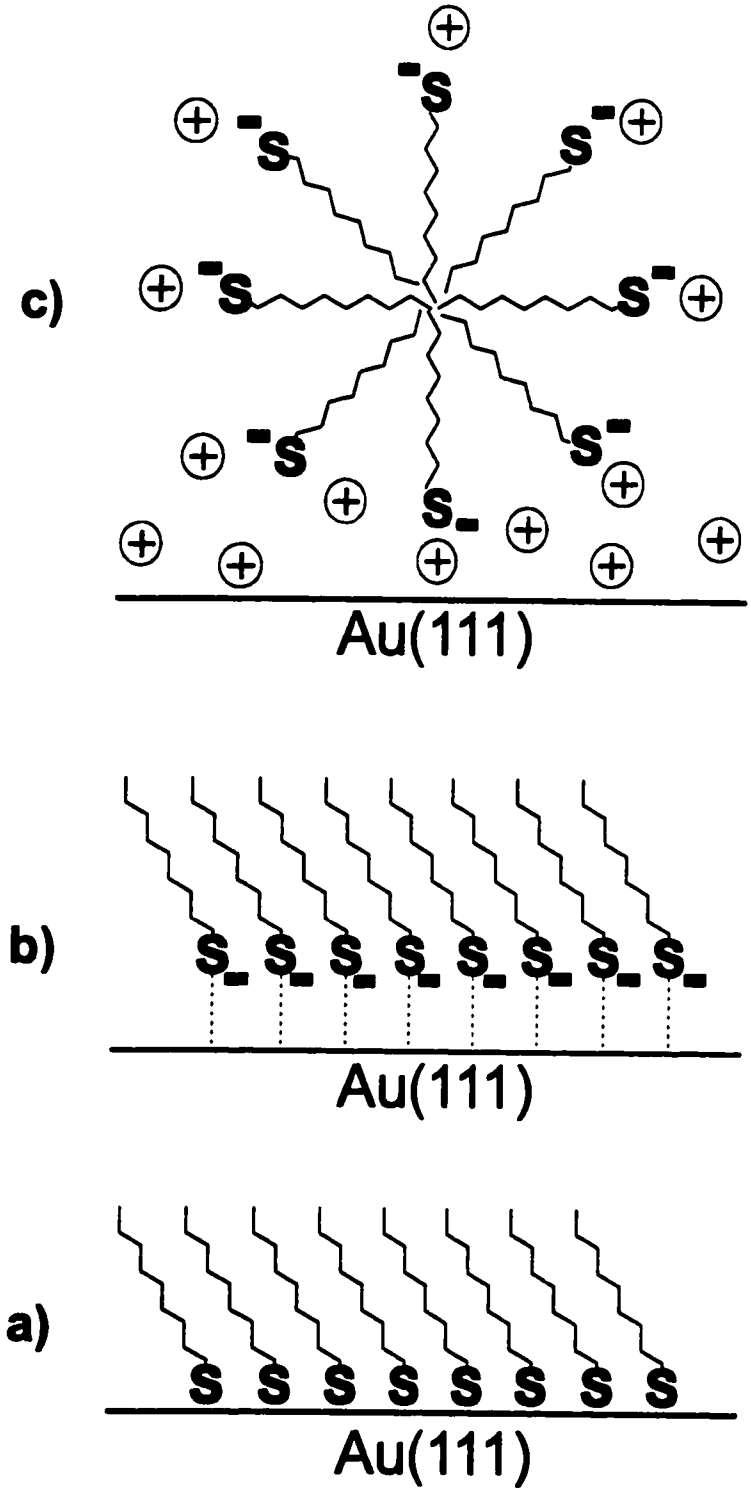

Figure 3.8: Proposed model for the repetitive reductive desorption/oxidative redeposition of a chemisorbed monolayer of low-solubility thiols. The reduction proceeds through the following steps: (a) chemisorbed thiols; (b) the reduction of the chemisorbed thiols creates the physisorbed thiolates, which form a lamellar structure; (c) when the potential is made more negative, physisorbed micelles of thiolates are formed. The oxidative redeposition proceeds through the reverse order of these steps.

B corresponds to going from the state in Figure 3.8(b) to the state in Figure 3.8(c).

The oxidative redeposition of the physisorbed micelles of thiolates proceeds by the same mechanism but in the reverse order. First, an electrospreading of the physisorbed micelles of thiolates occurs (going from Figure 3.8(c) to 3.8(b)). This happens between - 1.02 V and - 0.99 V, the potential range associated with peak B'. This step spreads the micelles of thiolates into a monolayer of thiolates. A positive capacitive current (corresponding to the current peak B') accompanies this reorientation of the thiolates due to the removal of the electrical double layer. Then, at potentials more positive than - 0.99V, the monolayer of physisorbed thiolates is oxidatively redeposited onto the Au(111) surface via a one-electron per molecule process (going from Figure 3.8(b) to 3.8(a)). This oxidative step is associated with peak A' and corresponds to the oxidative adsorption of an almost complete monolayer C16 (80-85 %; see section 3.1) . Only small changes in the IR intensity accompany this step. The structure and orientation of the electrodeposited monolayer are the same as in the initial monolayer.

The idea of the formation of micelles of thiolates is supported by many other studies [38-40]. Particularly, an in situ STM study has shown that aggregates with diameters from 3 to 12 nm form instantaneously when a C16/polycrystalline gold system is subjected to a potential of - 1.0 V [38]. The sizes and the heights of the aggregates increase when the potential is brought to - 1.2 V. The aggregates are ascribed to the formation of micelles of thiolates on the polycrystalline gold surface. The height of the aggregates suggests that spherical micelles are formed. When the thiolates are oxidatively redeposited, the aggregates disappear. This is compatible with our suggestion that a C16 monolayer can be reductively desorbed and oxidatively redeposited repetitively.

Finally, the mechanism that we propose for the reductive desorption and the oxidative redeposition of low-solubility thiols on Au(111) is similar to that observed for Langmuir-Blodgett monolayers of insoluble aliphatic alcohols and stearic acid on Au(111). Indeed, insoluble aliphatic alcohols and stearic acid have been found to repetitively desorb and redeposit onto Au(111) electrochemically [39,40]. It has also been shown that these Langmuir-Blodgett monolayers form physisorbed micelles at potential negative of the pzc of Au(111). At potentials positive of the pzc, the insoluble adsorbates form a physisorbed (lamellar) monolayer. These results support our suggestion that the peaks B and B' correspond to the potential induced transition of physisorbed thiolates from a lamellar arrangement to a micellar arrangement.

3.5 Summary:

In this chapter, we have seen that a monolayer of C16 on Au(111) can be reductively desorbed and oxidatively redeposited repetitively. This is due to the low solubility of C16 thiolates in an aqueous electrolyte solution. The C16 thiolates remain physisorbed on the Au(111) surface after their reductive desorption. This allows the subsequent oxidative redeposition of the thiolates. The average orientation (structure and order) of the alkane chains of a chemically deposited monolayer is preserved in the electrodeposited monolayer indicating that the transition from a chemisorbed state to a physisorbed state is reversible. The low solubility of C16 thiols also causes their reductive desorption and oxidative redeposition to occur in two steps: a faradaic step and a capacitive step. Our spectroelectrochemical results show that the first step in the reduction of a C16 monolayer is compatible with the reduction of most of the chemisorbed thiols. In this step, there is no substantial reorientation of the alkane chains. The second step of the reduction occurs at more negative

potentials and is ascribed to the formation of physisorbed micelles of thiolates. In this step, there is substantial reorientation of the alkane chains. This observation is concordant with the formation of micelles. The physisorbed thiolates are oxidatively redeposited through the reverse mechanism of the reduction. In light of this mechanism, we see that the faradaic reduction/oxidation of C16 thiols is decoupled from the formation/destruction of an electrical double layer because of the low solubility of the adsorbate. Finally, the electrochemical characteristics of insoluble thiols chemisorbed on Au(111) were found to be similar to those of Langmuir-Blodgett monolayers of insoluble adsorbates physisorbed on Au(111). This shows the important role that the solubility of the adsorbates plays in the electrodeposition of self-assembled organic monolayers.

CHAPTER 4: SHG Spectroscopy Results

In this chapter, we will present the in situ SHG spectroscopy results obtained for the reductive desorption and the oxidative redeposition of C16 on Au(111). This study of a weakly hyperpolarizable (C16) adsorbate on Au(111) using SHG spectroscopy was prompted by electrochemical evidence of a stabilization of the physisorbed C16 thiolates with time. We begin this chapter by presenting the electrochemical results.

Introduction:

4.1 Slow stabilization of physisorbed C16 thiolates on Au(111):

The in situ vibrational spectroscopy (SNIFTIRS) measurements of the previous section were obtained by taking the difference of two spectra measured at fixed potentials. Each of the spectra acquired at fixed potentials required 200 scans at a resolution of 2 cm^{-1} to obtain a good signal to noise ratio. Every spectrum took ~ 3 minutes to acquire for a total of ~ 6 minutes of acquisition time per SNIFTIRS spectrum. This corresponded to spending ~ 3 minutes in the physisorbed state of a C16 monolayer in each SNIFTIRS spectrum. The stability of a physisorbed C16 monolayer was confirmed for a period of 3 minutes via cyclic voltammetry, giving us confidence that the SNIFTIRS spectra are related to the current peaks in the cyclic voltammograms. The stability of a physisorbed C16 monolayer was also verified beyond a period of 3 minutes. In the cyclic voltammograms presented in Figure 4.1, the potential was scanned from -0.30 V to -1.30 V to reduce the chemisorbed C16 monolayer. On the subsequent positive going scan the potential was held at -1.05 V for 1, 5, and

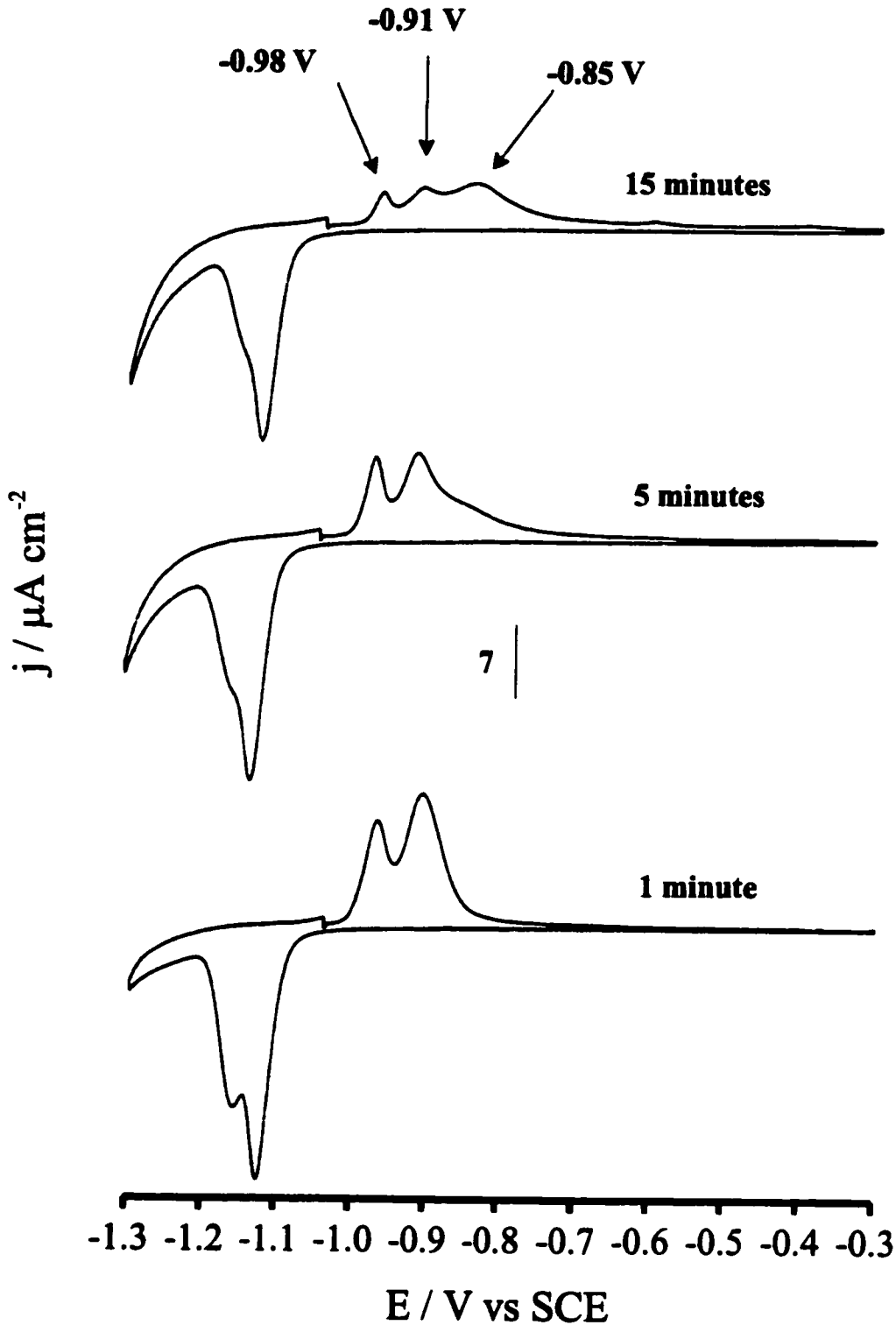

Figure 4.1: Changes in the stability of physisorbed C16 thiolates on Au(111) with time. The cyclic voltammograms were recorded as follows. The potential was scanned from - 0.30 V to - 1.30 V to reduce the C16 monolayer. On the subsequent positive scan, the potential was held at - 1.05 V for 1, 5, and 15 minutes before recording the oxidative redeposition.

15 minutes before recording the oxidative redeposition. After 5 minutes, we noticed a substantial decrease in the intensities of the peaks at -0.98 ± 0.01 V and -0.91 ± 0.01 V for the oxidative redeposition of C16 onto Au(111). In addition, a broad peak appears at a more positive potential of -0.85 ± 0.01 V. The charge integration of these three peaks is almost the same number as the charge integration for the reduction of the monolayer prior to the potential holding experiment at -1.05 V. Consequently, there is no substantial loss of thiols during the potential hold. After a period of 15 minutes, we see a decrease of the peaks at -0.98 ± 0.01 V and -0.91 ± 0.01 V and most of the oxidative redeposition charge integrates under the new peak at -0.85 ± 0.01 V. The appearance of a broad peak at a more positive potential of -0.85 ± 0.01 V suggests that it is harder to oxidatively redeposit the C16 monolayer onto Au(111) after holding the thiols in a physisorbed state. This stabilization of the physisorbed state of a C16 monolayer is a slow process, taking as much as 15 minutes to occur.

D. Yang et al. [17] have studied the effects of pH on the reductive removal and the oxidative redeposition of C16 on Au(111). Particularly, they observed that the oxidative redeposition peaks at -0.98 V and -0.91 V shift to more positive potentials and merge in one broad peak when the pH of the electrolyte was decreased. Between pH's 10.5 to 8.5, the oxidative redeposition voltammogram was characterized by a single broad peak at a potential ~ -0.80 V at pH 10.5 to ~ -0.70 V at pH 8.5. These changes occured at a pH close to the pK_a (10-12) for a thiol. Therefore, they ascribed the positive shift and merging of the two oxidative redeposition peaks to a reprotonation of the reduced thiols. This reprotonation adds the breaking of S-H bonds to the energetics of the redeposition thus increasing the potential required for the redeposition. We notice two important similarities between the study of D. Yang et al. and our results. First, the potential of the new peak formed after 15

minutes in the physisorbed state of a monolayer (~ -0.85 V), is close to the potential of the oxidative peak for pH's lower than 10.5, ~ -0.8 V. Second, the new peak that we observed at ~ -0.85 V is broad like the peak they observed at lower pH for the oxidative redeposition. This suggests that the physisorbed thiolates get protonated with time in our potential hold experiments. Indeed, voltammograms recorded after our potential hold experiments display the typical features of a C16/Au(111) cyclic voltammogram. This is an indication that the stabilization of the physisorbed state is a reversible process. Protonation is a reversible process. The protons may come from the bulk electrolyte by cation enrichment at the electrolyte/Au(111) interface in the presence of a negative electric field. However, since the pH is typically ~ 13 in our experiments, it is more likely that the protons come from the reductive decomposition of water molecules (hydrogen evolution). The onset of hydrogen evolution is ~ - 1.20 V in 0.1 M KOH on a clean Au(111) surface.

When alkanethiolates are protonated, they become neutral. It has been reported that neutral (non-charged) surfactants reduce their Gibbs surface energy by lying flat on the surface at potentials negative of the pzc of an electrode [41]. In the previous chapter, it was shown that the chemisorbed thiols, when reduced, go from a vertical arrangement of the alkane chains (with respect to the electrode surface) to a more horizontal arrangement (on average). Given that the protonation of physisorbed thiolates and the reduction of chemisorbed thiols cause the same change in the orientation of the alkane chains, protonation should increase the number of alkane chains that are lying horizontally with respect to the surface of Au(111) with time. In situ vibrational spectroscopy (SNIFTIRS) did not show changes in the orientation of the alkane chains of the physisorbed thiolates with time. The S-H stretching band in the 2600-2540 cm^{-1} region was not detected. However, the weakness of this IR-band [42], our sample size (nanomoles), and the surface selection rule at a metal

substrate's surface might have prevented its detection.

We have seen in CHAPTER 2 that SHG spectroscopy is sensitive to changes of the electronic hyperpolarizability of the surface of an electrode. The hyperpolarizability is dependent on the distribution of electrons. Molecules containing weakly bonded electrons such as ¶ electrons, negatively charged ions, and metals will display a detectable second harmonic signal [19]. The alkane chains of thiolates physisorbed on a gold surface are very weakly hyperpolarizable. The anionic head group S^- may be significantly hyperpolarizable compared to a protonated head group, S-H. Hence, the protonation of physisorbed thiolates could be monitored via changes in the intensity of the SHG signal coming from the interface of the C16/Au(111) system. The following sections present the variation of the SHG signal intensity with time for the reductive desorption and the oxidative redeposition of a C16 monolayer on Au(111). Section 4.2 presents the theory of the changes in the SHG signal intensity of the reductive and oxidative potential steps of the C16/Au(111) system. In section 4.3, we analyze SHG signal intensity changes observed on a time scale where the stabilization of the physisorbed state does not occur electrochemically (3 minutes). Finally, section 4.4 presents results obtained on a time scale where the stabilization of the physisorbed state occurs (15 minutes).

4.2 SHG theory for an electrochemical interface:

Relating changes in the intensity of SHG signals (I_{SHG}) to surface processes (adsorption, desorption, and surface reactions) requires knowledge of the different contributions to the total non linear susceptibility (χ_{tot}) at the interface (equation 4.1).

$$I_{SHG} \propto |\chi_{tot}|^2 \quad (4.1)$$

For an adsorbate/substrate system such as C16/Au(111), χ_{tot} can be separated in three contributions:

$$\chi_{tot} = \chi_{sub} + \chi_{int}(\theta(t)) + \chi_{ads}(\theta(t)) \quad (4.2)$$

χ_{sub} is the nonlinear susceptibility of the substrate, Au(111). χ_{int} is due to the interaction of the sulfur head group of C16 with the Au(111) surface (adsorbate/substrate interaction). χ_{ads} is the contribution from the alkane chains of the chemisorbed thiols. $\theta(t)$ is the time dependent coverage of the adsorbate. It is possible to obtain quantitative kinetic information on the surface processes if the relation between θ and the two non linear susceptibilities χ_{int} and χ_{ads} is known.

The simplest case arises when changes in χ_{tot} are proportional to changes in θ. The relative phases and maximum amplitudes of the different contributions to χ_{tot} determine the direction and the intensity of the total change in the SHG signal as the coverage varies. The relative phases and maximum amplitudes are not necessarily constant during a surface process. Changes of electronic resonances caused by the adsorption of thiols could modify the phases and amplitudes of the contributions to χ_{tot}. Consequently, a proportionality between χ_{tot} and θ cannot be assumed a priori. The relationship between the SHG signal and the adsorbate coverage must be verified experimentally.

Eisert [43] has shown that the phase relation between χ_{sub} and χ_{int} is constant and equal to 180° at λ_ω = 1064 nm for adsorbed thiols on gold. Buck et al. [20] neglected χ_{ads} in their studies of the spontaneous adsorption (absence of electric field) of alkanethiols onto gold substrates from various

incubation solutions because of the low hyperpolarizability of C-H bonds at λ_ω = 1064 nm. In a comparative study of SHG and XPS measurements [44], it was also established that the relationship between θ and χ_{int} is linear. The dependence of SHG intensity on the thiol coverage is given by:

$$I_{SHG} = A|\chi_{sub} + \chi_{int}^{(\theta=1)}\theta(t)|^2 (I_\omega)^2 \qquad (4.3)$$

A is a constant determined by the geometry of the experiment, the wavelength, and the dielectric constants [28]. I_ω is the intensity of the incoming fundamental beam. $\chi_{int}^{(\theta=1)}$ is the non linear susceptibility of the S-Au interaction for a complete monolayer. The 180° phase difference between χ_{sub} and χ_{int} causes a destructive interference between them.

The fact that a C16 monolayer remains physisorbed after its reductive desorption questions the validity of neglecting contributions from the reduced adsorbates in our experiments. We must introduce another contribution, $\chi_{phys}(\theta(t))$ to account for the hyperpolarizability of the negative sulfur head groups of the physisorbed C16 thiolates. Equation (4.3) becomes:

$$I_{SHG} = A|\chi_{sub} + \chi_{int}^{(\theta=1)}\theta(t) + \chi_{phys}(\theta(t))|^2 (I_\omega)^2 \qquad (4.4)$$

In equation (4.4), χ_{int} represents the contribution from the S-Au chemical bond and the residual electrostatic interaction of thiolates in close proximity to the surface after the the reduction of a C16 monolayer. The χ_{phys} term corresponds to the contribution from the hyperpolarizable sulfur head groups of physisorbed thiolates. The direction of the changes of χ_{phys} and its variation with coverage must be determined experimentally.

Under conditions where χ_{sub} is constant, equation (4.4) would apply. However, in our experiments, the substrate is electrochemically subjected to different potentials. The electronic density at the substrate's surface may change substantially [19]. χ_{sub} is then modified by a dc-field term:

$$\chi_{eff} = \chi_{sub} + E_{dc}\, \chi_{dc/\omega} \qquad (4.5)$$

χ_{eff} is the non linear susceptibility of the substrate subjected to a static dc-field. E_{dc} is the static dc-field applied. $\chi_{dc/\omega}$ is the non linear susceptibility for the coupling of the dc-field with the electromagnetic field at frequency ω.

Results and discussion:

4.3 The reversible reduction/oxidation of C16 on Au(111):

In order to interpret the results obtained for the reductive desorption and the oxidative redeposition of C16 on Au(111) with SHG spectroscopy, it is imperative that we first determine the contributions of the substrate and the adsorbate to the total SHG signal.

In Figure 4.2(g), the SHG signal coming from a clean Au(111) surface was monitored with time while the potential of the substrate jumped between -0.30 V (corresponding to the chemisorbed state of a C16 monolayer) and -1.20 V (corresponding to the physisorbed state of a C16 monolayer). The experiments were conducted in an S-S polarized configuration (see CHAPTER 2). The SHG signal was acquired at -0.30 V for the first 2.5 minutes to establish a baseline. The potential was then

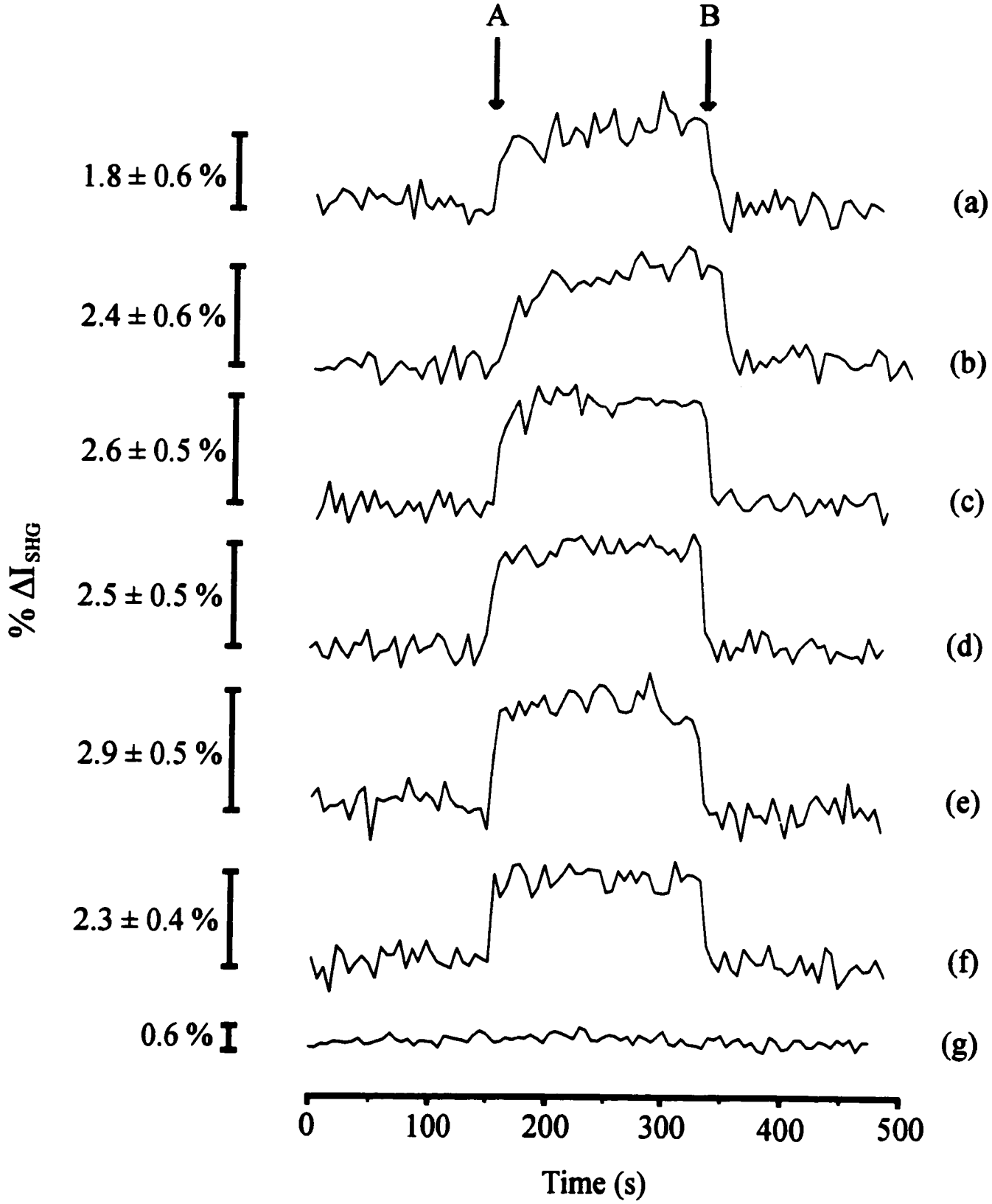

Figure 4.2: % variation of the SHG signal intensity with time for:
(a) to (e): the reduction and the oxidation of C16 on Au(111). The reductive potential steps (A) were from - 0.30 V to (a) - 1.12 V, (b) - 1.14 V, (c) - 1.16 V, (d) - 1.18 V, and (e) - 1.20 V. In each case, we waited 3 minutes before jumping back to - 0.30 V (B).
(f): the reduction and the oxidation of C4 on Au(111). The reductive potential step (A) was from - 0.30 V to - 1.00 V. We waited 3 minutes before jumping back to - 0.30 V (B).
(g): a blank experiment. The potential of a clean Au(111) surface was jumped from - 0.30 V to - 1.20 V (A), and held at - 1.20 V for 3 minutes. Then, the potential was jumped back to - 0.30 V (B).
Each trace ((a) to (g)) is an average of 10 traces. Each data point of the individual traces used for signal averaging is an average of 10 sums of 5 laser shots.

jumped from -0.30 V to -1.20 V and held there for 3 minutes, after which the potential was brought back to -0.30 V. No changes in the intensity of the SHG signal were observed outside the noise (± 0.3 %). We carried out similar experiments for different polarization configurations (P-S, P-P, and S-P) and the changes observed in the SHG signal intensity were also negligeable. In other words, χ_{sub} » $E_{dc}\,\chi_{dc/\omega}$ and $\chi_{eff} \approx \chi_{sub}$. Hence the substrate's contribution (surface reconstructions and changes of the electronic density distribution) to the total non linear susceptibility can be assumed constant with potential in 0.1 M KOH electrolyte.

Depicted in Figures 4.2 (a) to (e) are the SHG signal intensity changes with time for the reductive desorption and the oxidative redeposition of C16 on Au(111) via different potential steps (- 0.3 V to potentials between - 1.12 V and - 1.20 V). The experiments were carried out in the same fashion as the blank experiment described in the previous paragraph. In all cases, we observe a quasi instantaneous change of the SHG signal intensity when the potential is jumped between two values. When the potential step is negative going, the monolayer gets reduced and we observe an increase in the SHG signal. A positive going potential step oxidatively redeposits the monolayer and we observe an equal decrease in the SHG signal back to its value before the reductive potential step. The percentage change (whenever this term is used, we mean the percentage change with respect to the baseline value acquired initially at - 0.30 V) of the SHG signal intensity observed for potential steps to - 1.16 V, - 1.18 V, and - 1.20 V remains constant (within the noise) and equals on average to a change of 2.7 ± 0.2 % during the 3 minutes at these potentials. For potential steps to - 1.12 V and - 1.14 V, the percentage change in the SHG signal intensity increases slightly and gradually during the 3 minutes at these potentials. Thus, the average percentage change observed for steps to - 1.12 V and - 1.14 V are 1.8 ± 0.6 % and 2.4 ± 0.6 % respectively. At - 1.12 V and - 1.14 V, the

percentage changes level off after 3 minutes to values that overlap the average value (2.7 ± 0.2 %) observed for potential steps to - 1.16 V, - 1.18 V, and - 1.20 V. Consequently, we may conclude that the percentage change in the SHG signal intensity is the same for all potential steps after 3 minutes. However, it levels off more slowly for potential steps to - 1.12 V and - 1.14 V.

To determine the contribution of χ_{phys} (physisorbed thiolates) to the SHG signal intensity changes in Figures 4.2 (a) to (e), we looked at the reductive desorption and the oxidative redeposition of 1-butanethiol (C4) on Au(111). C4 is soluble in a 0.1 M KOH electrolyte. Hence, a monolayer of C4 will not remain physisorbed at the electrolyte/Au(111) interface upon its reductive desorption. A contribution from a physisorbed state will not be possible for this system. Since the 3s and 3p energy levels of sulfur are the same for alkanethiols of different chain lengths, the interaction of C4 with the Au (111) (χ_{int}) surface should be equivalent to that of C16. The only difference between the C4/Au(111) and the C16/Au(111) systems will be the presence (or not) of physisorbed thiolates at the electrolyte/substrate interface. The preparation of a C4 monolayer was carried out as follows. The C4 monolayer was electrodeposited from the electrolyte solution which contained 10^{-3} M of C4. This was done by bringing the clean Au (111) substrate in contact with the electrolyte solution at a potential of - 0.30 V (potential where a C4 monolayer is chemisorbed) for a few seconds. The presence of C4 in the electrolyte solution also permitted the oxidative redeposition of C4 onto the substrate. Figure 4.3 displays the cyclic voltammogram of C4 on Au(111) resulting from this preparation. Upon the negative going scan, the C4 monolayer gets reduced at - 0.89 ± 0.01 V. We observe the oxidative redeposition of the C4 monolayer upon the positive going scan at - 0.78 ± 0.01 V. We based the choice of our potential steps used for the SHG spectroscopy experiments on these cyclic voltammetry results. In Figure 4.2(f), the SHG signal intensity of a C4 covered Au(111) surface

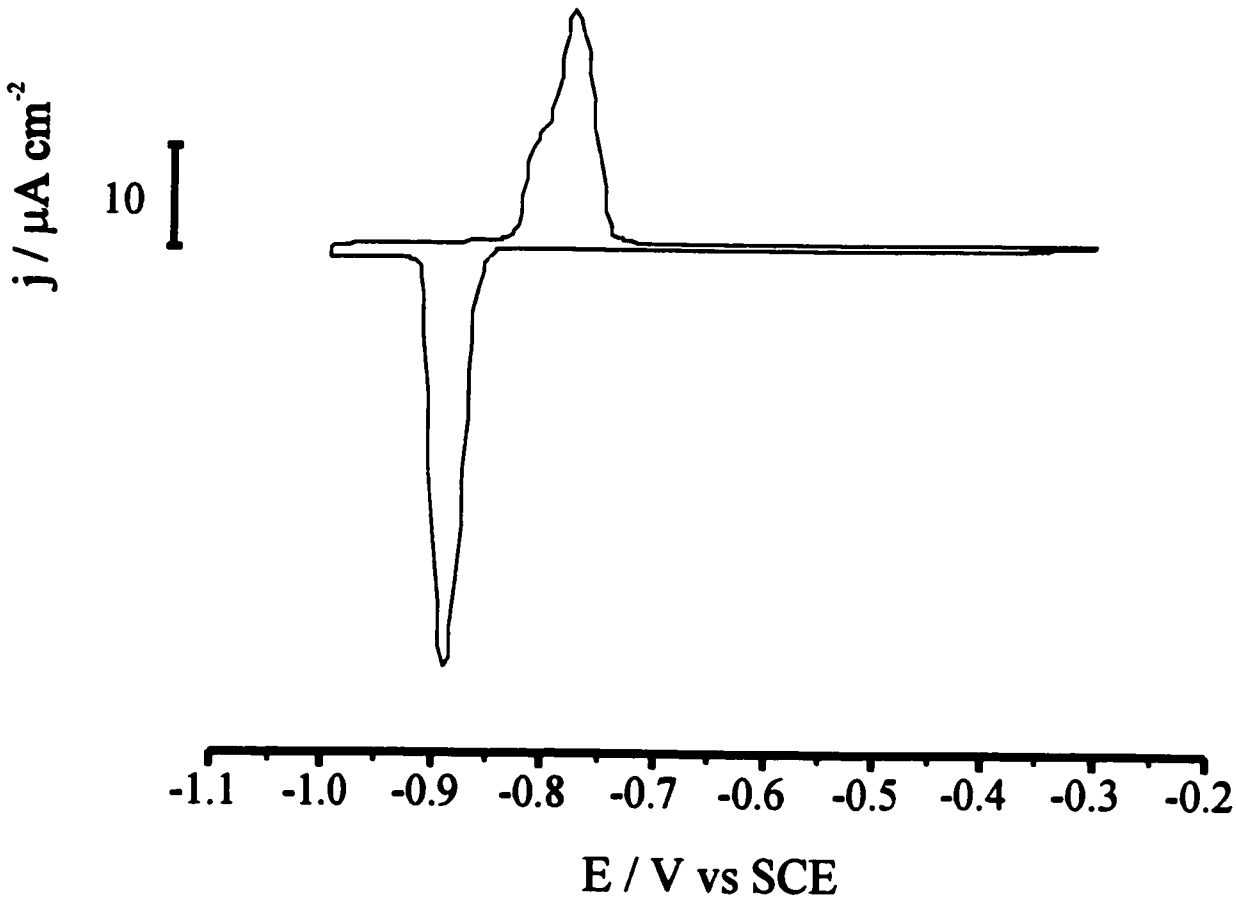

Figure 4.3: Cyclic voltammogram obtained when the Au(111) surface is immersed in an electrolyte solution of 0.1 M KOH containing 10 mM of 1-butanethiolates. The scan rate was 20 mV s^{-1}.

was monitored with time while the potential jumped between - 0.30 V (corresponding to the C4 covered Au(111) surface) and - 1.00 V (corresponding to the clean Au(111) surface). The experiments were carried out in the same fashion as the blank experiment reported above. We observe the same changes of the SHG signal intensity with time as for C16 (i.e. the quasi instantaneous increase and decrease of the SHG signal intensity for negative and positive going steps respectively). The percentage change of the SHG signal intensity is constant (within the noise) and equals on average 2.3 ± 0.4 % for the 3 minutes at - 1.00 V. We see that this change is identical to the change observed for C16 (2.7 ± 0.2 %). This may be accounted for in one of two ways. First, if χ_{phys} is assumed negligeable, we fall back to equation (4.3) suggested by Buck et al. [20] to describe the SHG signal intensity coming from alkanethiol/gold systems. It follows that the SHG signal intensity changes are due to the S-Au interaction only. Thus the changes observed for C4 and C16 are expected to be identical. If χ_{phys} is assumed non-zero for physisorbed C16 thiolates, equation 4.4 will apply for the C16/Au(111) system whereas equation (4.3) will apply for the C4/Au(111) system. Then, the changes observed for C4 and C16 may be identical only if the decrease of the χ_{int} term (due to the breaking of the S-Au bond) for the C16/Au (111) system is smaller than the decrease of the χ_{int} term for the C4/Au(111) system and that the χ_{phys} term of the C16/Au (111) system compensates by an amount equal to the difference: $\Delta\chi_{int}$(C4) - $\Delta\chi_{int}$(C16). It follows that χ_{phys} must have a constructive phase and a magnitude that varies with the reductive and oxidative potential steps. We note that the phase does not have to be constant, as long as it is within a constructive range. In reality, the C16 monolayer is not desorbed from the surface upon a reductive potential step. Therefore, it is not improbable that the χ_{int} of a C16/Au(111) system decreases less than that of the C4/Au(111) system due to some residual interaction of thiolates in close proximity of the surface (the change is not complete compared with the C4/Au(111) system). Indeed the proximity of negatively

charge species (physisorbed thiolates) will make the substrate's surface more positive and less hyperpolarizable. On the other hand, the formation of physisorbed thiolates produces negatively charged sulfur head groups which should be more hyperpolarizable than sulfur head groups bound to the surface. Thus it is not improbable that an increase in the SHG signal intensity be caused by the χ_{phys} term to compensate for the difference: $\Delta\chi_{int}(C4) - \Delta\chi_{int}(C16)$.

Based on the previous discussion, we interpret the SHG spectroscopy results obtained for the C16/Au(111) system as follows. The slow increase of the SHG signal intensity observed during the 3 minute hold at - 1.12 V and - 1.14 V is accounted for by a reorientation of the physisorbed thiolates. Figure 3.7 from CHAPTER 3 shows that - 1.12 V and - 1.14 V are within a potential range associated mostly with the reorientation of physisorbed thiolates (peak B of the reductive desorption voltammogram of C16 on Au(111)). Furthermore, we see (Figure 3.7) that the reorientation of the physisorbed thiolates is not complete at - 1.12 V and - 1.14 V. We observe a similar incompleteness of the percentage changes of the SHG signal intensity for potential jumps to - 1.12 V and - 1.14 V at the start of the 3 minute holding period. Thus, we believe that a small part of the changes in the SHG signal intensity could be caused by the slow reorientation of physisorbed thiolates. This interpretation is compatible with the suggestion that χ_{phys} could be non-zero for the physisorbed thiolates. We will present more evidence in the next section that χ_{phys} is non-zero. The quasi instantaneous increase of the SHG signal intensity accompanying negative going potential jumps is ascribed to the breaking of the S-Au bond (the faradaic reduction of the chemisorbed C16 molecules) and the creation of thiolates. Finally, we associate the quasi instantaneous decrease of the SHG signal intensity accompanying positive going potential jumps with the adsorption of thiolates and the formation of the S-Au bond (the faradaic oxidation of physisorbed thiolates). These quasi

instantaneous changes of the non linear optical properties at the substrate's surface with the potential jumps agree with chronoamperometric studies [36] which indicate that the faradaic reduction and oxidation of C16 on Au(111) occur in a second or less. The direction of the SHG signal intensity changes for the positive and negative going potential jumps agrees with the qualitative predictions of equation 4.4 and is also compatible with SHG results reported for the adsorption of alkanethiols onto gold substrates from ethanolic solutions [4,20,21] (i.e. adsorption causes a decrease in SHG signal intensity). When the S-Au interaction is broken, electrons at the interface become more delocalized, thus causing an increase in the hyperpolarizability of the interface (and vice versa).

4.4 The stabilization of physisorbed thiolates:

Following the methodology used previously, we will begin this section by presenting a blank experiment. This blank experiment was carried out as follows. The SHG signal was acquired at -0.30 V for the first 5 minutes to establish a baseline. The potential was then jumped from -0.30 V to -1.20 V and held there for ~15 minutes, after which the potential was brought back to -0.30 V. This experiment is shown in Figure 4.4. We observed no changes in the SHG signal intensity outside the noise (± 0.5 %). SHG signal intensity changes were also negligeable for the other polarization configurations (P-S, P-P, and S-P). Thus, $\chi_{sub} \gg E_{dc}\, \chi_{dc/\omega}$ and $\chi_{eff} \approx \chi_{sub}$. We may assume that the substrate's contribution (surface reconstructions and changes of the electronic density distribution) to the total nonlinear susceptibility is constant in this range of potentials.

Figure 4.5 presents a typical trace of the changes in the SHG signal intensity observed with time when a C16 monolayer is reductively desorbed and held in its physisorbed state at - 1.20 V for longer

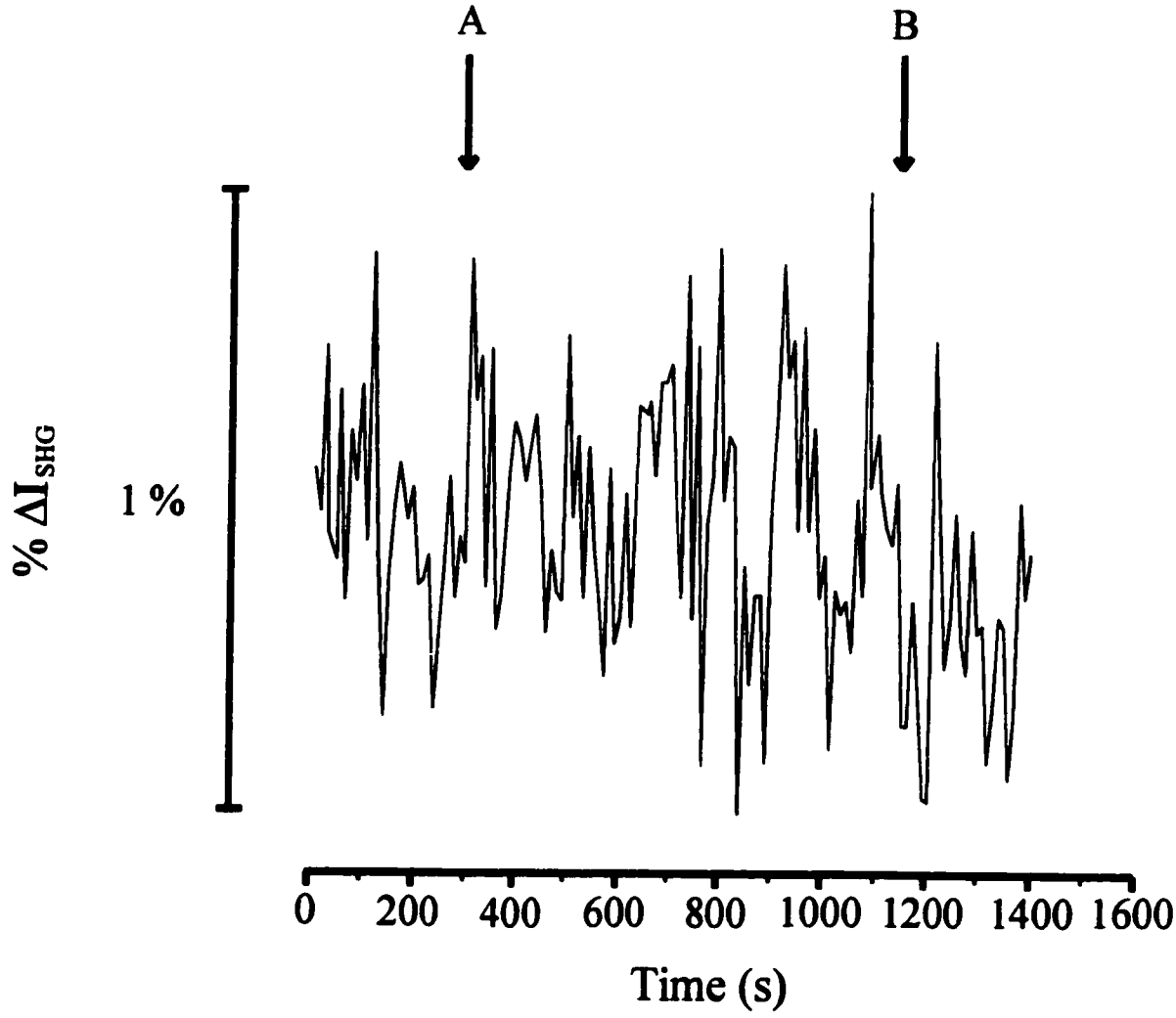

Figure 4.4: % variation of the SHG signal intensity with time for a blank experiment. The potential of a clean Au(111) surface was jumped from - 0.30 V to - 1.20 V (A) and held at - 1.20 V for 15 minutes. Then it was jumped back to - 0.30 V (B). Each data point in the SHG signal trace is an average of 10 sums of 10 laser shots.

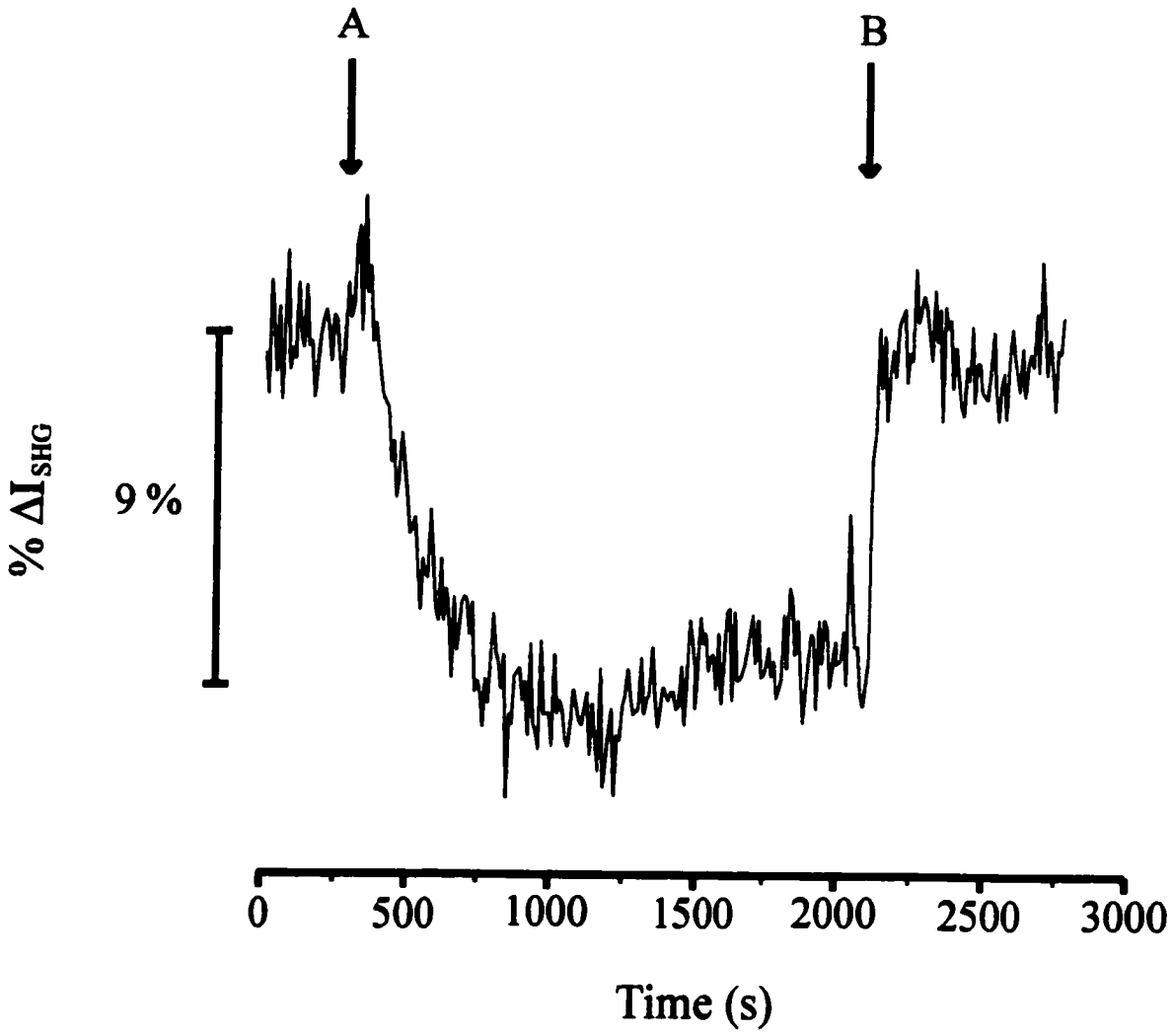

Figure 4.5: % variation of the SHG signal intensity with time for the reduction and the oxidation of C16 on Au(111). The reductive potential step (A) was from - 0.30 V to - 1.20 V. We waited 30 minutes before jumping back to - 0.30 V (B). Each data point in the SHG signal trace is an average of 10 sums of 10 laser shots.

than 3 minutes. The experiment was carried out in the same fashion as the blank experiment described in the previous paragraph. However, the potential hold at - 1.20 V lasted 30 minutes rather than 15 minutes. These 30 minutes were necessary for the signal to reach a stable value. When the potential is jumped from - 0.30 V to - 1.20 V, we observe a quasi instantaneous increase in the SHG signal intensity of ~ 2.5 %. During the first 3 minutes at - 1.20 V, the SHG signal intensity remains constant. This is similar to what we have seen for the corresponding short time experiment. Beyond 3 minutes, the SHG signal intensity decreases exponentially by ~ 9 % and then levels off after 15 minutes. Upon the potential jump from - 1.20 V to - 0.30 V, the SHG signal intensity rapidly (within a minute) increases back to the initial baseline value. This experiment was repeated 10 times. We found that the percentage decrease observed beyond 3 minutes ranges from 9 % to 59 %. The shape of the decrease is complex. However the time scale of the decrease is always around 15 minutes. Upon the oxidative redeposition of the monolayer, the SHG signal may recover as much as 100 % or as little as 15 % of the initial baseline intensity. The increase upon the oxidative redeposition is not always as rapid as in Figure 4.5. Similar results were observed for potential jumps to - 1.18 V and - 1.22 V. Figures 4.6 and 4.7 display two traces for the jump to - 1.22 V that illustrate, along with Figure 4.5, the variability of the percentage changes of the intensity of the SHG signal observed from experiment to experiment. This variability seems to be intrinsic to the system under study. Indeed, much care was taken in controlling the experimental conditions (see Theory and Experiment Section). For potential jumps to values between - 1.14 V and - 1.12 V, we observe a much slower percentage decrease beyond 3 minutes such that after the 30 minutes at these potential values, the percentage decrease is very small. This is illustrated by the trace in Figure 4.8 obtained for a potential jump to - 1.14 V. We note that - 1.14 V is in the potential range where, for short time experiments (previous section), a slow reorganization of the physisorbed thiolates is suggested to occur.

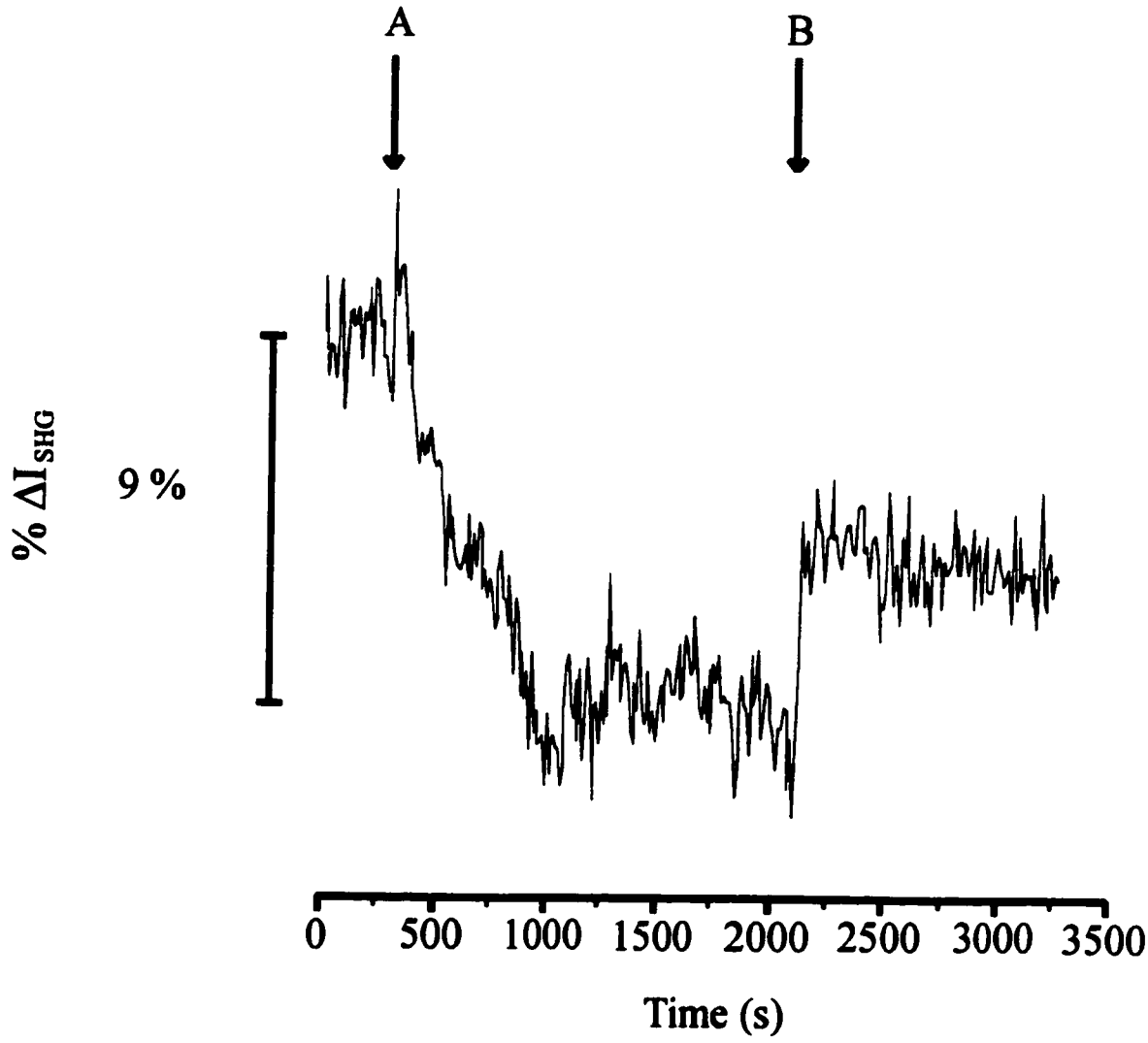

Figure 4.6: % variation of the SHG signal intensity with time for the reduction and the oxidation of C16 on Au(111). The reductive potential step (A) was from - 0.30 V to - 1.22 V. We waited 30 minutes before jumping back to - 0.30 V (B). Each data point in the SHG signal trace is an average of 10 sums of 10 laser shots.

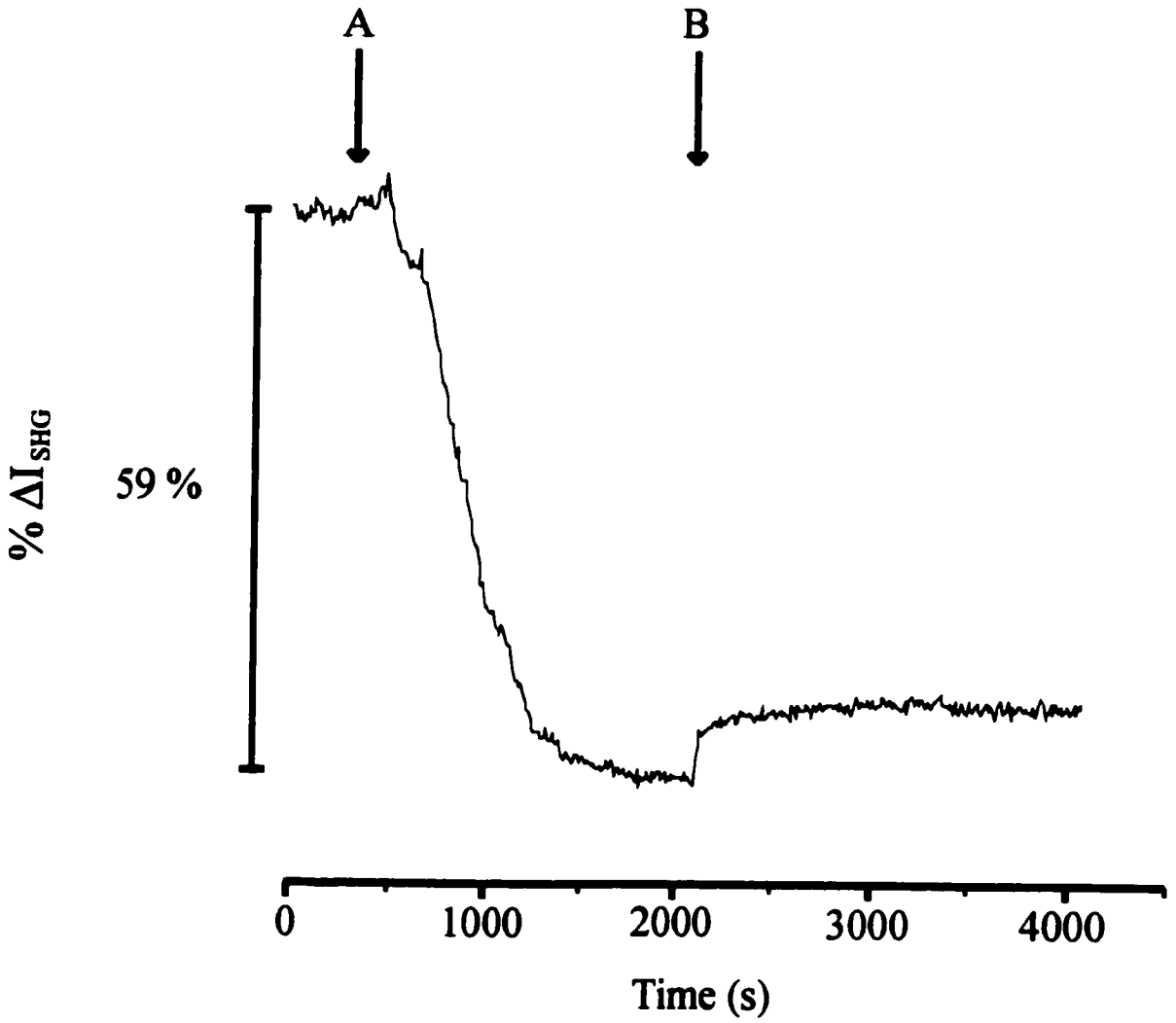

Figure 4.7: % variation of the SHG signal intensity with time for the reduction and the oxidation of C16 on Au(111). The reductive potential step (A) was from - 0.30 V to - 1.22 V. We waited 30 minutes before jumping back to - 0.30 V (B). Each data point in the SHG signal trace is an average of 10 sums of 10 laser shots.

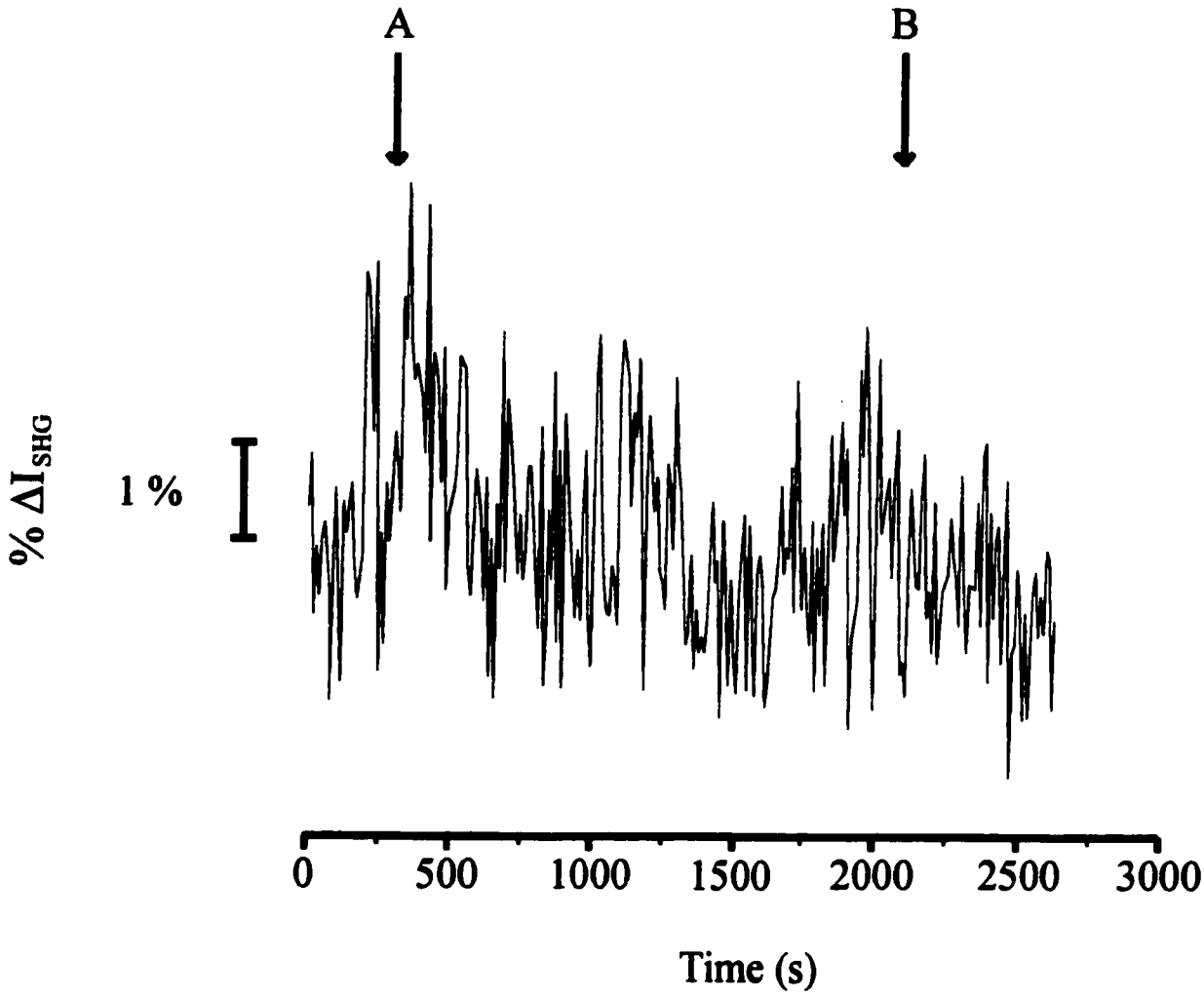

Figure 4.8: % variation of the SHG signal intensity with time for the reduction and the oxidation of C16 on Au(111). The reductive potential step (A) was from - 0.30 V to - 1.14 V. We waited 30 minutes before jumping back to - 0.3 V (B). Each data point in the SHG signal trace is an average of 10 sums of 10 laser shots.

The changes of the SHG signal intensity observed in Figures 4.5, 4.6, and 4.7 were verified against similar experiments using the C4/Au(111) system. These experiments were carried out as follows. The SHG signal was acquired at -0.30 V for the first 5 minutes to establish a baseline. The potential was then jumped from -0.30 V to -1.00 V and held there for ~15 minutes, after which the potential was brought back to -0.30 V. These experiments are summarized in Figure 4.9. We observe the same changes of the SHG signal intensity with time as for the short time C4 experiments whenever the potential is jumped between - 0.30 V and - 1.00 V. During the 15 minutes at - 1.00 V, the SHG signal intensity remains constant at ~ 2.5 %. The same results were obtained when the potential was jumped to - 1.20 V and - 1.22 V and held at these values for 30 minutes (see Figures 4.10 and 4.11). This comparative study between the C16/Au(111) and the C4/Au(111) systems demonstrates that the presence of physisorbed thiolates at the substrate's surface is the cause of the changes of the SHG signal intensity after 3 minutes at the most negative potential in Figures 4.5, 4.6, and 4.7. Hence we conclude that χ_{phys} is non-zero for physisorbed alkanethiolates.

When the C16 thiolates are physisorbed for long periods of time (over 3 minutes), some molecules are lost to the bulk electrolyte. The changes observed after 30 minutes in the physisorbed state could be due to this loss of molecules. However, experiments with the soluble C4 presented in the previous paragraph show that the maximum percentage change that can be observed for the complete removal of an alkanethiol monolayer is ~ 2.5 %. This percentage change is much smaller compared with the percentage changes observed for a C16 monolayer held in its physisorbed state for more than 3 minutes. If part of the changes in the SHG signal intensity in Figures 4.5, 4.6, and 4.7 are due to the loss of molecules to the bulk electrolyte, the contribution is clearly less than 2.5 %. The changes in the SHG signal intensity in Figures 4.5, 4.6, and 4.7 were observed for a loss of molecules as small

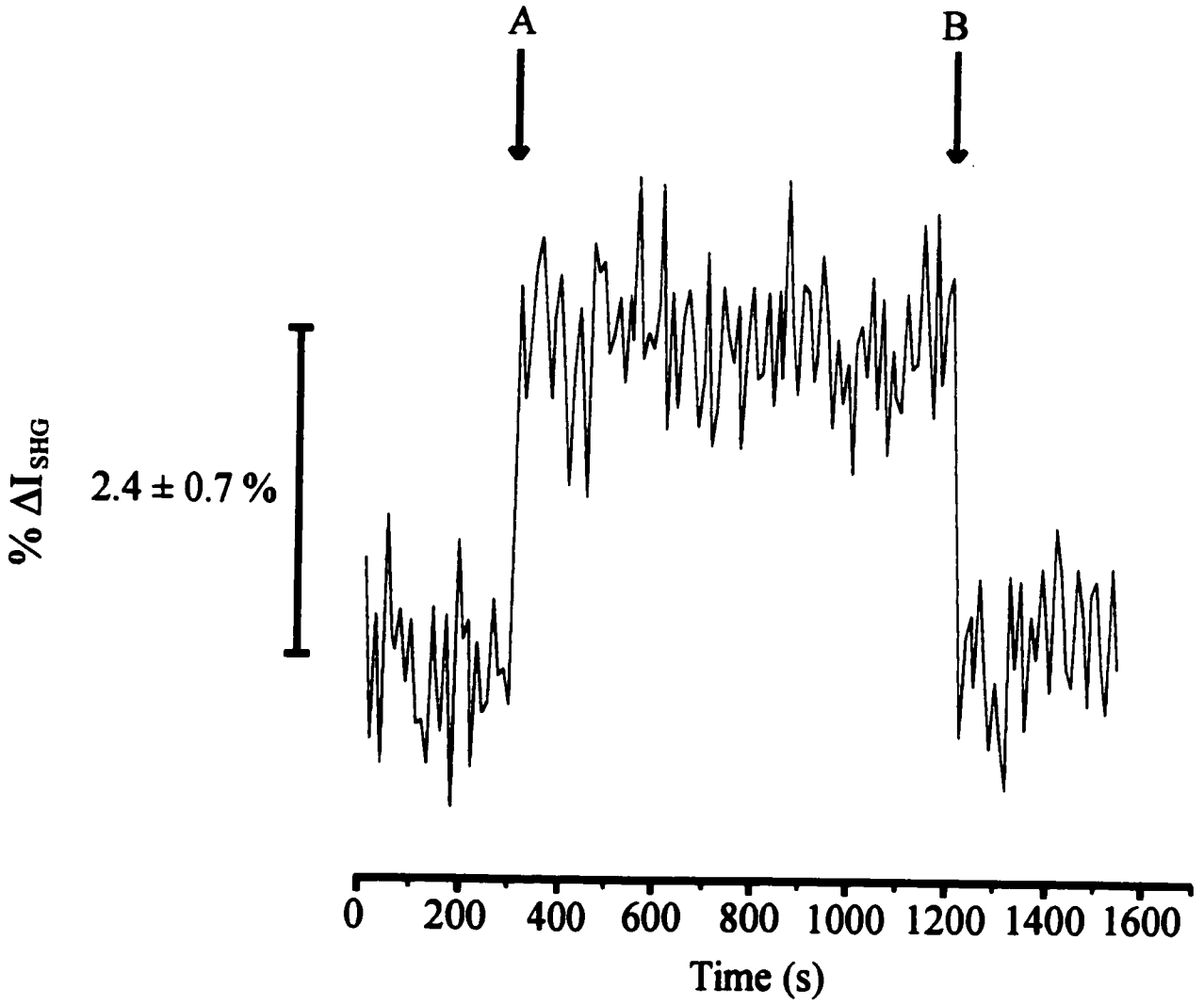

Figure 4.9: % variation of the SHG signal intensity with time for the reduction and the oxidation of C4 on Au(111). The reductive potential step (A) was from - 0.30 V to - 1.00V. We waited 15 minutes before jumping back to - 0.30 V (B). Each data point in the SHG signal trace is an average of 10 sums of 10 laser shots.

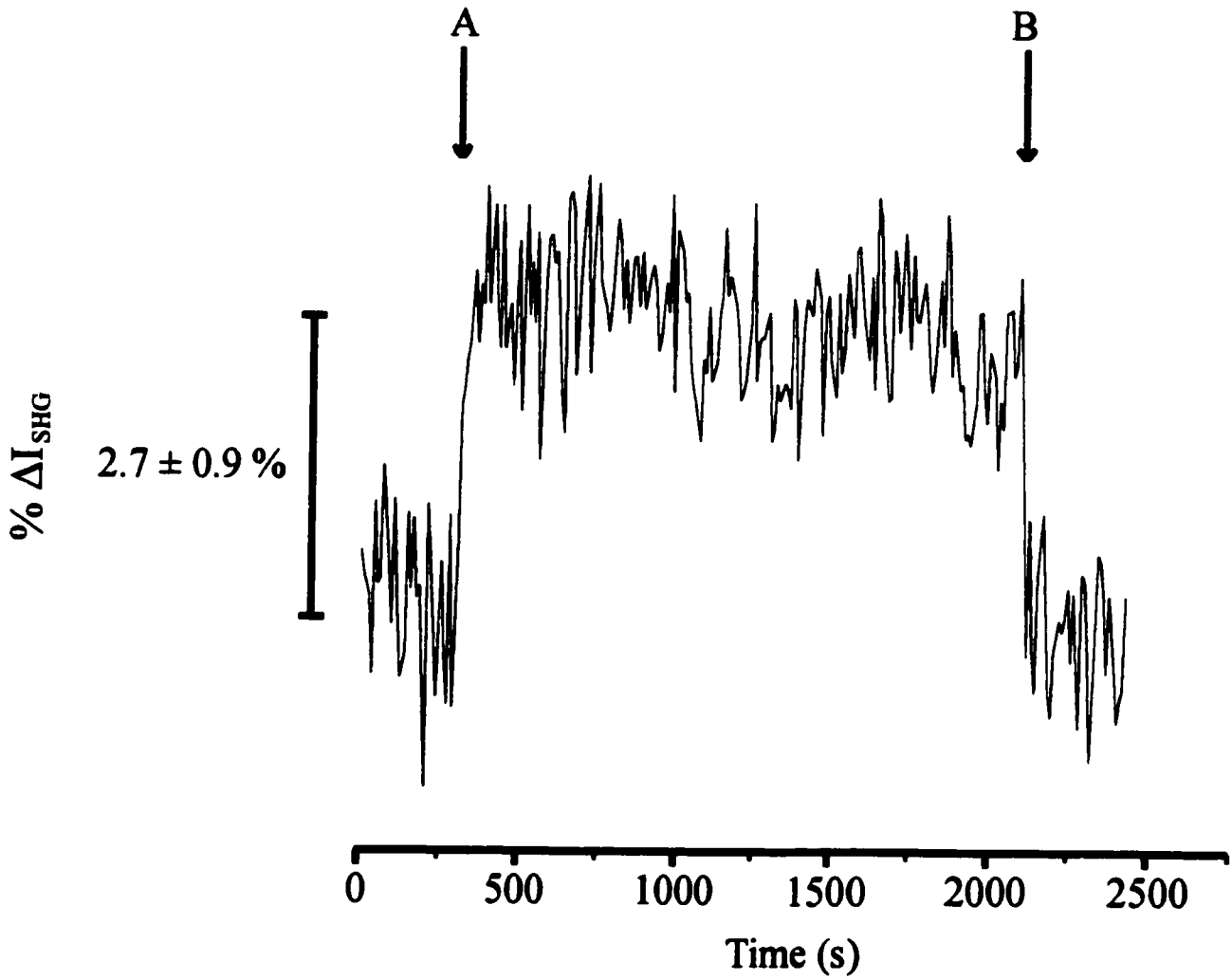

Figure 4.10: % variation of the SHG signal intensity with time for the reduction and the oxidation of C4 on Au(111). The reductive potential step (A) was from - 0.30 V to - 1.20 V. We waited 30 minutes before jumping back to - 0.30 V (B). Each data point in the SHG signal trace is an average of 10 sums of 10 laser shots.

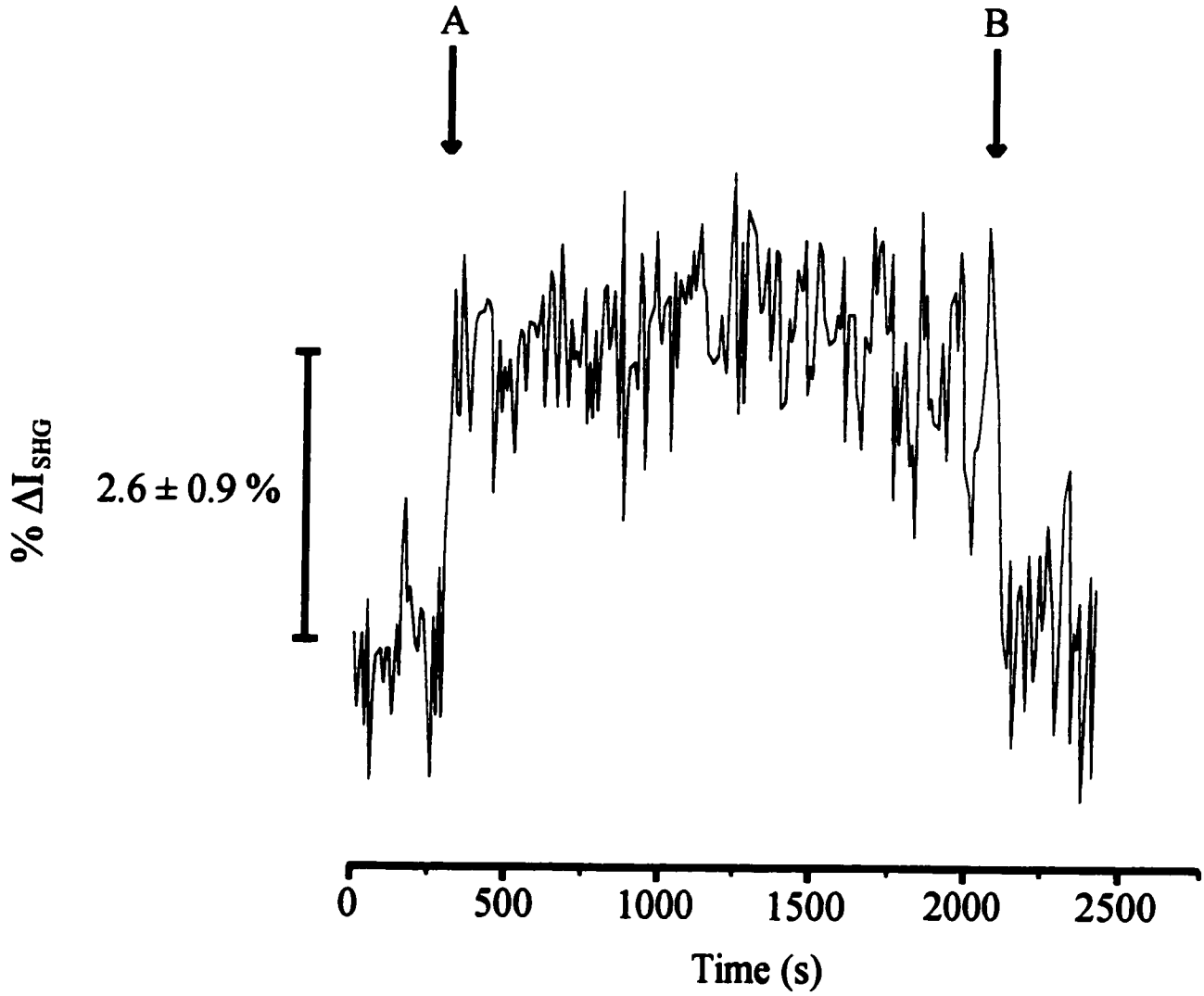

Figure 4.11: % variation of the SHG signal intensity with time for the reduction and the oxidation of C4 on Au(111). The reductive potential step (A) was from - 0.30 V to - 1.22 V. We waited 30 minutes before jumping back to - 0.30 V (B). Each data point in the SHG signal trace is an average of 10 sums of 10 laser shots.

as ~ 2 % of a monolayer. This means that any changes due to the loss of molecules would be within the noise of our measurements ~ ± 0.5 % (2 % of 2.5 % is 0.05 %). It is important to mention here that on certain days, we have observed similar changes in the SHG signal intensity to those in Figures 4.5, 4.6, and 4.7 for a loss of molecules as large as ~ 40 % of a monolayer. This indicates that the relation between the coverage and both χ_{phys} and χ_{int} is not linear. Thus, the equation we have introduced in section 4.2 to express the SHG signal intensity should be rewritten as follows:

$$I_{SHG} = A|\chi_{sub} + \chi_{int}(\theta(t)) + \chi_{phys}(\theta(t))|^2 (I_\omega)^2 \qquad (4.6)$$

where we no longer assume a linear relation between the coverage and χ_{int}.

4.5 Origin of the slow stabilization of physisorbed C16 thiolates:

We ascribe the decrease of the SHG signal intensity observed when thiolates are held in a physisorbed state for more than 3 minutes to a protonation process. Indeed, the time scale on which this SHG signal intensity drop occurs (~ 15 minutes) is comparable with the time scale on which the electrochemical stabilization of physisorbed C16 thiolates takes place. According to the experimental evidence presented in section 4.1, the electrochemical stabilization of physisorbed C16 thiolates is due to a protonation process. It is reasonable that a protonation of physisorbed thiolates should decrease the SHG signal intensity since the hyperpolarizable electrons of the negatively charged sulfur head groups become localized into a S-H bond. The idea that the physisorbed thiolates undergo a chemical transformation is supported by the differences between the traces of the SHG signal intensity for short time (Figure 4.2 (e)) and long time (Figure 4.5) experiments. More importantly, we note that upon

the oxidative redeposition of C16 on Au(111), the SHG signal intensity increases for long time experiments whereas it decreases for short time experiments. This is a strong indication of a chemical transformation of physisorbed thiolates.

At this point, it may seem unlikely that a protonation of physisorbed thiolates should cause such a large change in the SHG signal intensity since we only observe a small ~ 2.5 % change for the complete removal of an alkanethiol monolayer from the substrate's surface. However, by acknowledging that the phases and magnitudes of χ_{int} and χ_{phys} may not be the same, it becomes plausible to have large differences of the percentage changes of the SHG signal intensity caused by the physisorbed thiolates (χ_{phys}) and the S-Au interaction (χ_{int}).

Buck et al. [4] have used SHG spectroscopy to study the adsorption of 12-(4-nitroanilino)dodecanethiol on polycrystalline gold from ethanol and n-hexane. They found that the adsorption process involves a slow organization of the p-nitroaniline endgroups involving the expulsion of the solvant molecules. The organization takes ~ 20 minutes in ethanol and as much as 133 minutes in n-hexane. This organization causes large changes in the SHG signal intensity in both solvents. In ethanol, the signal increases by a factor of 10. In n-hexane, it increases by a factor of 7. They also report variations of the phase of the nonlinear susceptibility contribution of the p-nitroaniline endgroups with respect to that of the substrate. These results support our suggestion that a hyperpolarizable group in close proximity to our Au(111) substrate (the negative sulfur head groups of thiolates), when chemically transformed, may cause large changes in the SHG signal intensity due to variations (or differences) between the phases of χ_{phys} and the other nonlinear susceptibility contributions.

The source of protons in the long time experiments depicted in Figures 4.5, 4.6, and 4.7 may be from the bulk electrolyte or from hydrogen evolution as mentioned in section 4.1. We have estimated the total number of protons present in 7 mL (the capacity of our spectroelectrochemical cell) of 0.1 M KOH and found it insufficient to account for the protonation of a whole monolayer of C16 thiolates (there is ~ $7.0*10^5$ times more thiolates than protons). Cation enrichment at the electrolyte/substrate interface in the presence of a negative electric field may change the pH at the substrate's surface by a few orders of magnitude. If the pH becomes low enough at the most negative potentials of our experiments, it may be possible to protonate some physisorbed thiolates via this route. In order to protonate all physisorbed thiolates via the cation enrichment route, it is understood that an amount greater than the available supply of protons in 0.1 M KOH will have to be provided by bulk water molecules. This implies a displacement of the proton/hydroxide equilibrium towards the formation of protons to replenish the proton depletion in the bulk electrolyte. When protons are abundant in the bulk electrolyte, the protonation of physisorbed thiolates should be a fast spontaneous process (given the pKa of thiols ~ 10-12). However, for a 0.1 M bulk KOH concentration, the displacement of the proton/hydroxide equilibrium may be difficult, thus causing a slow protonation of physisorbed thiolates. In this fashion, the protonation of physisorbed thiolates via the cation enrichment route could explain the slow kinetics observed experimentally. On the other hand, hydrogen evolution is an efficient source of protons under the experimental conditions that we used throughout this study. This was verified with a simple calculation using the Butler-Volmer equation and the known limiting current density for hydrogen evolution on the surface of a gold substrate. This calculation revealed that thousands of monolayers of hydrogen are formed per second per square centimeter at the potentials of our experiments. It has been suggested [45] that hydrogen evolution in alkaline solutions proceeds via the adsorption and subsequent decomposition of water molecules

on metal surfaces:

$$M(e) + H_2O \rightarrow MH + OH^- \qquad (4.7)$$

Given the efficiency of hydrogen evolution under our experimental conditions, the 15 minute decrease in the the SHG signal intensity we observe for long time experiments must be due to the protonation step and not to the formation of hydrogen. We can explain why such an efficient proton source would not protonate the physisorbed thiolates rapidly by considering the fact that the hydrogen atoms, when formed, are temporarily chemisorbed at the metal surface and undergo rapid reaction with a neighboring hydrogen to form hydrogen gas. In this respect, the protonation of thiolates would be in competition with rapid hydrogen evolution. Also, it is not obvious how the negatively charged sulfur head groups of thiolates should approach the negatively charged surface of Au(111) to bind with a hydrogen atom. This process is further complicated by the fact that protonation of thiolates will make them neutral. Neutral thiols at a negatively charged metal surface will lie flat on the surface [41], thus blocking the surface and making any subsequent protonation more difficult.

The variability of the results obtained for long time experiments (wide range of percentage changes of the SHG signal intensity from one experiment to another, etc ...) best fits with a protonation process caused by hydrogen evolution. Indeed, hydrogen evolution on gold substrates was shown to be sensitive to the surface structure [46]. Thus, the number and position of surface defects should influence the efficiency of hydrogen evolution across the substrate's surface. For long time experiments, when the reductive potential jump is made to potentials further away from hydrogen evolution, the decrease in the SHG signal intensity slows down (see Figure 4.8). This also supports

the idea of a protonation process via hydrogen evolution. Consequently, hydrogen evolution seems to be the most likely source of protons for the protonation process observed experimentally.

4.6 Summary:

On a time scale when the stabilization of the physisorbed state of a C16 monolayer on Au(111) does not occur electrochemically (3 minutes), it was possible to observe the reversible reductive desorption/oxidative redeposition of C16 on Au(111) through changes in the nonlinear optical properties at the electrolyte/substrate interface. Indeed, we found that the changes in the SHG signal intensity with potential steps are mainly due to the S-Au interaction. There is possibly a small contribution from the reorientation of physisorbed thiolates. The SHG signal intensity changes for reductive (and oxidative) potential steps to very negative (or positive) potentials follow the charge changes associated with the potential steps. In this respect, the C16/Au(111) system presents some potential as an optical switch. Also, if the reduction potential applied to C16/Au (111) is positive enough, it would be possible to look at the kinetics of the reduction process. Our SHG spectroscopy results support the assignment of the stabilization of physisorbed thiolates to a protonation process. The mechanism for this protonation process seems to involve hydrogen evolution rather than cation enrichment at the substrate's surface. Kinetics of the protonation process could not be extracted from these long time experiments because of the variability of our results. This variability seems to be intrinsic to the the system under study. Indeed, if hydrogen evolution is the proton source for the protonation process, then the kinetics are expected to be variable.

CHAPTER 5: Conclusion

We have presented a new mechanism for the reductive desorption and the oxidative redeposition of low-solubility alkanethiols on Au(111) in an alkaline electrolyte solution. This mechanism explains the origin of the two current peaks in the reductive and oxidative voltammetric waves observed by cyclic voltammetry for low-solubility thiols/Au(111)/alkaline electrolyte systems. The low solubility of the long alkane chain thiols (alkane chains with more than 12 carbons) was found to be the cause for this two-step mechanism. The mechanism is described in Figure 5.1. In the cyclic voltammogram of C16 on Au(111) in 0.1 M KOH (Figure 3.1(a)), current peak A is assigned to an almost complete faradaic reduction of all the chemisorbed thiols into a monolayer of physisorbed thiolates (going from Figure 5.1(a) to (b). The unblocking of the Au(111) surface caused by the destruction of the monolayer of physisorbed thiolates (formation of micelles of thiolates) at more negative potentials and which allows the formation of an electrical double layer (going from Figure 5.1(b) to (c)), is assigned to the capacitve current peak B. If we remain in the state of physisorbed micelles of thiolates (Figure 5.1(c)) for longer than 3 minutes, the thiolates undergo a slow (15 minutes) stabilization that is most probably caused by a slow protonation process occuring at negative potentials. The source of the protons is most likely from hydrogen evolution. The oxidative redeposition of physisorbed micelles of thiolates proceeds via the electrospreading of the micelles into a lamellar arrangement (going from Figure 5.1(c) to (b)). This step is assigned to current peak B'. The faradaic oxidation of the thiolates into chemisorbed thiols follows. This faradaic oxidation corresponds to current peak A'. It is important to mention that this mechanism can explain the presence of only one broad peak at more positive potentials in the oxidative redeposition voltammogram of protonated thiolates. If the thiolates are neutralized by protonation they will no longer experience a strong electrostatic driving

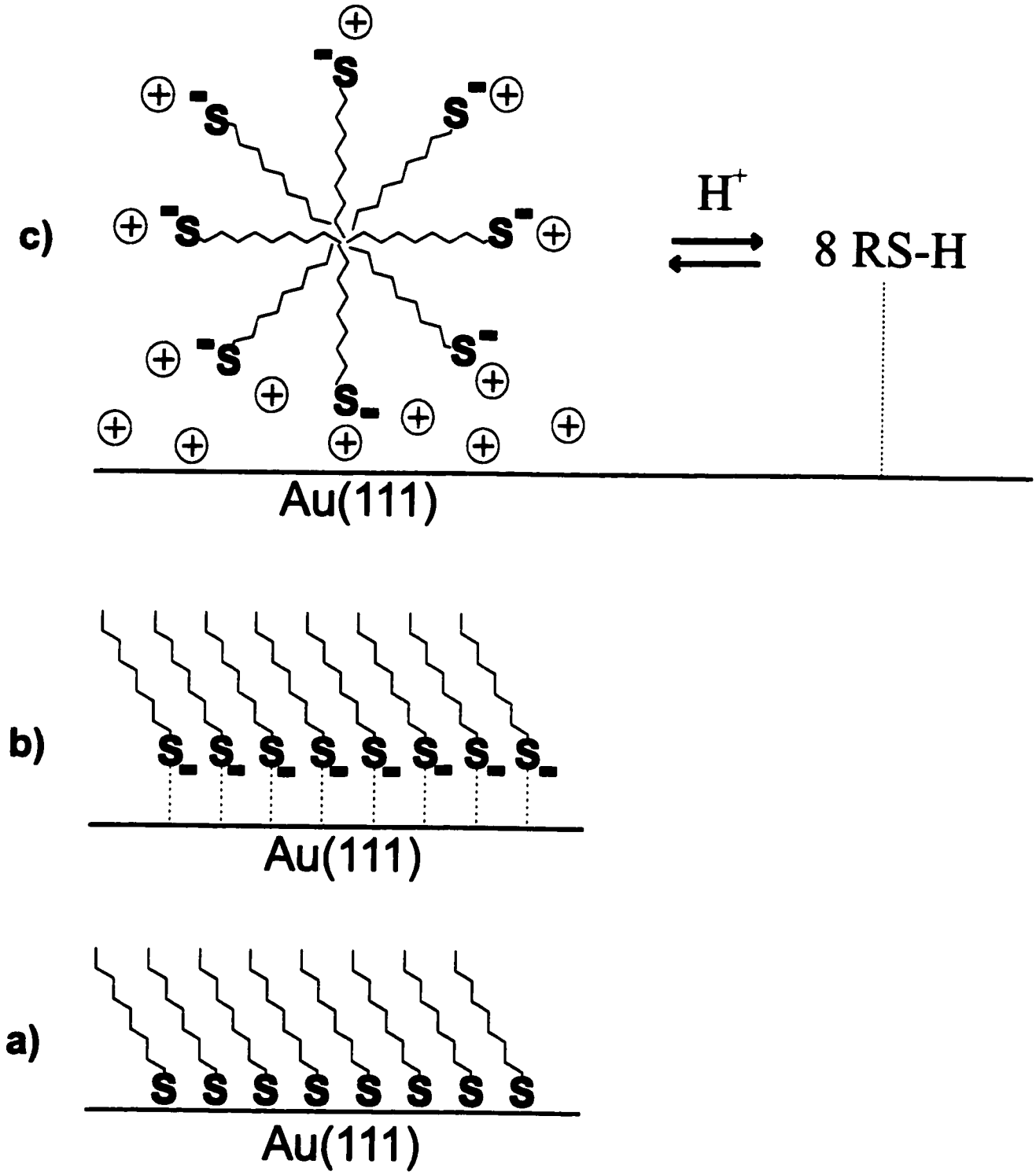

Figure 5.1:Proposed model for the repetitive reductive desorption/oxidative redeposition of a chemisorbed monolayer of low-solubility thiols. The reduction proceeds through the following steps: (a) chemisorbed thiols; (b) the reduction of the chemisorbed thiols creates the physisorbed thiolates, which form a lamellar structure; (c) when the potential is made more negative, physisorbed micelles of thiolates are formed. If we maintain the thiolates in the micellar state (c), a reversible protonation occurs after 3 minutes. The oxidative redeposition proceeds through the reverse order of these steps.

force in the electrospreading (capacitive current peak B') step. The capacitive peak could then decrease in intensity, shift to more positive potentials and collapse with the faradaic step (current peak A'). The breaking of the S-H bond would also add itself to the energetics of the oxidative redeposition and this could shift current peak A' to more positive potentials. The similarity between the electrochemical characteristics of insoluble thiols chemisorbed on Au(111) and those of Langmuir-Blodgett monolayers of insoluble adsorbates physisorbed on Au(111) shows the important role that the solubility of the adsorbates plays in the electrodeposition of self-assembled organic monolayers. Finally, on a time scale when the stabilization of the physisorbed state of a C16 monolayer on Au(111) does not occur electrochemically (3 minutes), changes in the SHG signal intensity coming from a C16/Au(111) system were found to follow the charge observed during the potential steps. In this respect, the C16/Au(111) system presents some potential as an optical switch. For potential steps to less negative potentials, the kinetics of the reduction process of C16 on Au(111) seems to be accessible via SHG spectroscopy.

N. B.: A part of the results presented in this thesis have been published [49,50].

References

[1] Ulman, A. *An introduction to ultrathin organic films from Langmuir-Blodgett to self-assembly*; Academic Press, INC.: New York, 1991.

[2] Fruböse, C.; Doblhofer, K. *J. Chem. Soc. Faraday Trans.* **1995**, 91(13), 1949.

[3] Bain, C. D.; Troughton, E. B.; Tao, Y. T.; Evall, J.; Whitesides, G. M.; Nuzzo, R. G. *J. Am. Chem. Soc.* **1989**, 111, 321.

[4] Dannenberger, O.; Wolff, J. J.; Buck, M. *Langmuir* **1998**, 14, 4679.

[5] Creager, S. E.; Olsen, K. G. *Anal. Chim. Acta* **1995**, 307, 277.

[6] Prime, K. L.; Whitesides, G. M. *J. Am. Chem. Soc.* **1993**, 115, 10714.

[7] Porter, M. D.; Bright, T. B.; Allara, D. L.; Chidsey, C. E. D. *J. Am. Chem. Soc.* **1987**, 109, 3559.

[8] Hahner G.; Woll, Ch.; Buck, M.; Grunze, M. *Langmuir* **1993**, 9, 1955.

[9] Bensebaa, F.; Voicu, R.; Huron, L.; Ellis, T. H. *Langmuir* **1997**, 13, 5335.

[10] Ishida, T.; Tsuneda S.; Nishida, N.; Hara, M.; Sasabe, H.; Knoll, W. *Langmuir* **1997**, 13, 4638.

[11] Weisshaar, D. E.; Lamp, B. D.; Porter, M. D. *J. Am. Chem. Soc.* **1992**, 114, 5860.

[12] Hatchett, D. W.; Uibel, R. H.; Stevenson, K. J.; Harris, J. M.; White, H. S. *J. Am. Chem. Soc.* **1998**, 120, 1062.

[13] Hatchett, D. W.; Stevenson, K. J.; Lacy, W. B.; Harris, J. M.; White, H. S. *J. Am. Chem. Soc.* **1997**, 119, 6596.

[14] Stevenson, K. J.; Mitchell, M.; White, H. S. *J. Phys. Chem. B* **1998**, 102, 1235.

[15] Schneider, T. W.; Buttry, D. A. *J. Am. Chem. Soc.* **1993**, 115, 12391.

[16] Zhing, C. J.; Porter, M. D. *J. Electroanal. Chem.* **1997**, 425, 147.

[17] Yang, D.; Wilde, C. P.; Morin, M. *Langmuir* **1997**, 13, 243.

[18] Yang, D.; Wilde, C. P.; Morin, M. *Langmuir* **1996**, 12, 6570.

[19] Brevet, P.-F. *Surface second harmonic generation*; Presses polytechniques et universitaires romandes: France, 1997.

[20] Dannenberger, O.; Buck, M.; Grunze, M. *J. Phys. Chem. B* **1999**, 103, 2202.

[21] Buck, M.; Grunze, M. *J. Vac. Sci. Technol. A* **1992**, 10(4), 926.

[22] Yang, D.; Al-Maznai, H.; Morin, M. *J. Phys. Chem. B* **1997**, 101, 1158.

[23] Hamelin, A. In *Modern Aspects of Electrochemistry*; Conway, B. E., White, R. E., Bockris, J. O'M., Eds.; Plenum Press: New York, 1985; Vol. 16, Chapter 1.

[24] Yang, D.; Lipkowski, J. *Langmuir* **1994**, 10, 2647.

[25] Woodruff, D. P.; Delchar T. A. *Modern techniques of surface science*; Cambridge University Press: Great Britain, 1992.

[26] Friedrich, A.; Pettinger, B.; Kolb, D. M.; Lupke, G.; Steinhoff, R.; Marowsky, G. *Chem. Phys. Lett.* **1989**, 163, 123.

[27] Svelto, O. *Principles of Lasers*; edited by D. C. Hanna, Plenum: New York, 1989.

[28] Shen, Y. R. *The principles of nonlinear optics*; Wiley: New York, 1984.

[29] Widrig, C. A.; Chung, C.; Porter, M. D. *J. Electroanal. Chem.* **1991**, 310, 335.

[30] Nuzzo, R. G.; Dubois, L. H.; Allara, D. L. *J. Am. Chem. Soc.* **1990**, 112, 558.

[31] Stole, S. M.; Porter, M. D. *Langmuir* **1990**, 6, 1199.

[32] Gatin, M.; Anderson, M. R. *Langmuir* **1994**, 10, 1638.

[33] Greenler, R. G. *J. Chem. Phys.* **1996**, 44, 310.

[34] Chidsey, C. E. D.; Liu, G. Y.; Rowntree, P.; Scoles, G. J. *J. Chem. Phys.* **1989**, 91, 4421.

[35] Sellers, H.; Ulman, A.; Shnidman, Y.; Eilers, J. E. *J. Am. Chem. Soc.* **1993**, 115, 9389.

[36] Yang, D.; Morin, M. *J. Electroanal. Chem.* **1998**, 441, 173.

[37] Tanford, C. *The hydrophobic effect: Formation of micelles and biological membranes*; Wiley: New York, 1980.

[38] Koichiro, D. H.; Miyake, K.; Imabayashi, S. I.; Niki, K.; Kakiuchi, T. *Langmuir* **1998**, 14, 3590.

[39] Bizzotto, D.; Lipkowski, J. *Prog. Surf. Sci.* **1995**, 50, 237.

[40] Bizzotto, D.; Noël, J. J.; Lipkowski, J. *J. Electroanal. Chem.* **1994**, 369, 259.

[41] Cachet, C.; Keddam, M.; Mariotte, V.; Wiart, R. *Electrochimica Acta* **1994**, 39(18), 2743.

[42] Silverstein, R. M.; Bassler, G. Clayton; Morrill, Terence C. *Spectrometric identification of organic compounds*; Wiley: New York, 1991.

[43] Eisert, F. Ph.D. Thesis, University of Heidelberg, 1993.

[44] Buck, M.; Eisert, F.; Fischer, J.; Grunze, M.; Träger, F. *Appl. Phys. A* **1991**, 53, 552.

[45] Bockris, J. O'M.; Reddy, A. K. N. *Modern electrochemistry (Volume 2)*; Plenum/Rosetta: New York, 1977.

[46] Perez, J.; Gonzalez, E. R.; Villullas, H. M. *J. Phys. Chem. B* **1998**, 102, 10931.

[47] Bard, A. J.; Faulkner, L. R. *Electrochemical methods: Fundamentals and applications*; Wiley: New York, 1980.

[48] Morin, Sylvie, *Study of the Adsorption of Pyridine on Silver Single Crystal Electrodes*, M. Sc. thesis, University of Guelph, Ontario, **1991**.

[49] Byloos, M.; Al-Maznai, H.; Morin, M. *J. Phys. Chem. B* **1999**, 103, 6554.

[50] Byloos, M.; Al-Maznai, H.; Qu, D.; Mohtat, N.; Morin, M. In *New Directions in Electro-*

analytical Chemistry II; Leddy, J., Vanysek, P., Porter, M. D., Eds.; The Electrochemical Society, Inc.: U.S.A., 1999; Vol. 99-5, p. 236.